

Optimized Strong Stability Preserving IMEX Runge–Kutta Methods

Inmaculada Higuera^{a,1,*}, Natalie Happenhofer^{b,3,4}, Othmar Koch^{c,2}, Friedrich Kupka^{b,2,4}

^a*Universidad Pública de Navarra, Departamento de Ingeniería Matemática e Informática, Campus de Arrosadia, 31006 Pamplona, Spain*

^b*University of Vienna, Faculty of Mathematics, Nordbergstraße 15, A-1090 Wien, Austria*

^c*Vienna University of Technology, Institute for Analysis and Scientific Computing, A-1040 Wien, Austria*

Abstract

We construct and analyze robust strong stability preserving IMPLICIT–EXPLICIT Runge–Kutta (IMEX RK) methods for models of flow with diffusion as they appear in astrophysics, and in many other fields where equations with similar structure arise. It turns out that besides the optimization of the region of absolute monotonicity, some other properties of the methods are crucial for the success of such simulations. In particular, the models in our focus dictate to also take into account the step size limits associated with dissipativity, positivity of the stiff parabolic terms which represent transport by diffusion, the uniform convergence with respect to different stiffness properties of those same terms, etc. Furthermore, in the literature, some other properties, like the inclusion of a part of the imaginary axis in the stability region, have been argued to be relevant.

In this paper, we construct several new IMEX RK methods which differ from each other by taking various or even all of these constraints simultaneously into account. It is demonstrated for some simple examples as well as for the problem of double–diffusive convection, that the newly constructed schemes provide a significant computational advantage over other methods from the literature. Due to their accumulation of different stability properties, the optimized IMEX RK methods obtained in this paper are robust schemes that may also be useful for general models which involve the solution of advection–diffusion equations, or other transport equations with similar stability requirements.

Keywords: Runge–Kutta, implicit–explicit, strong stability preserving, total variation diminishing, IMEX, SSP, TVD, numerical methods, hydrodynamics, double–diffusive convection, stellar convection and pulsation.

2000 MSC: 65L05, 65M06, 65M08, 65M20

1. Introduction

In this paper we discuss the construction of optimized strong stability preserving (SSP) implicit–explicit (IMEX) Runge–Kutta (RK) methods. The original motivation for this work is the need of robust schemes in radiation hydrodynamical simulations which are common in various fields of astrophysics. Specifically, the associated models of flow and radiative transport inside stars have the structure of advection–diffusion equations which can be discretized in space by dissipative finite difference methods and essentially non–oscillatory (ENO) schemes, and subsequently propagated in time by efficient time stepping methods.

In this context, due to the complexity of the problem, implicit time stepping methods cannot be used, but on the other hand, explicit time integration schemes are extremely inefficient. For these reasons, IMEX

*Corresponding author.

¹Supported by the Ministerio de Ciencia e Innovación, project MTM2011–23203.

²Supported by the Austrian Science Fund (FWF), project P21742.

³Supported by the Austrian Science Fund (FWF), project P20973.

⁴Supported by the Austrian Science Fund (FWF), project P25229.

strategies are preferred. IMEX methods require an additive splitting of the differential system, and thus we consider initial value problem for additive ordinary differential equations (ODEs) of the form

$$\dot{y}(t) = F(y(t)) + G(y(t)), \quad y(0) = y_0, \quad (1)$$

where we assume that the vector fields F and G have different stiffness properties.

In [21], *additive Runge–Kutta schemes* were demonstrated to improve the efficiency of numerical simulations for the semiconvection problem in astrophysics. In this reference, the methods were constructed with the aim to optimize the *region of absolute monotonicity*. This region characterizes the step sizes which are admissible in order to ensure that the total variation (or some other suitable sublinear functional) of the spatial profile does not increase artificially in the course of time integration [11, 30]. In the case of the total-variation seminorm, this property is commonly referred to as *total variation diminishing (TVD)* or, more generally, as *strong stability preserving (SSP)* (see, for example, [4, 5, 26]). In [21], it was demonstrated that for the solution of the semiconvection problem, TVD IMEX methods from the literature provide a significant computational advantage and enhance the stability and accuracy of the simulations. However, the IMEX RK methods available do not possess some other properties which are also beneficial to astrophysical simulations.

Motivated by these observations, the aim of the present paper is to construct new schemes which have additional properties at the cost of reducing the region of absolute monotonicity from the optimum. An analysis of the properties of TVD IMEX RK methods available in the literature and experimental assessment of their performance in the context of numerical simulations in astrophysics, see [21], indicates that the following properties of the methods promise reliable and efficient simulations:

- The IMEX RK scheme should be of second order. Furthermore, the error constant should be small. Since the accuracy of such simulations is generally limited by the spatial resolution, third order methods do not promise further advantages.
- The IMEX RK scheme should be SSP and it should have a large region of absolute monotonicity [11, 12]. This implies that both the explicit and the implicit schemes are SSP. Furthermore, the Kraaijevanger’s coefficient, also known as the radius of absolute monotonicity (see [19]), of both schemes should also be large.
- The stability function of the implicit scheme should tend to zero at infinity, and the stability region should contain a large subinterval of the negative real axis $[-z, 0]$, with $z > 0$. This is ensured by L -stability.
- For the explicit scheme, the stability region should contain large subintervals of the negative real axis, $[-z, 0]$, with $z > 0$, and also of the imaginary axis, $[-iw, iw]$, with $w > 0$. The latter requirement is associated with a stable integration of the hyperbolic advection terms (see [23, 32]).
- For both schemes, the stability function should be nonnegative for a large interval of the negative real axis, $[-z, 0]$, with $z > 0$. This condition is directly related to the step size restrictions associated with the dissipativity of the spatial discretization [31], and should prevent spurious oscillations of the numerical solution.
- The region of absolute stability of the IMEX RK scheme should be large.
- For a convenient and memory-efficient implementation, the coefficients of the scheme should be rational numbers which could enable to recombine the stages in a suitable way.

The properties listed above turn out to be more important for a successful simulation than third order accuracy. Still, we cannot use the optimal second order two-stage method in [21], because the number of

degrees of freedom does not allow to have a positive stability function in conjunction with L -stability. Thus, we will focus on the construction of second-order three-stage IMEX RK schemes $(\mathcal{A}, \tilde{\mathcal{A}}, b^t)$ of the form:

$$\begin{array}{c|ccc}
 0 & 0 & 0 & 0 & \tilde{c}_1 & \gamma & 0 & 0 \\
 c_2 & a_{21} & 0 & 0 & \tilde{c}_2 & \tilde{a}_{21} & \gamma & 0 \\
 c_3 & a_{31} & a_{32} & 0 & \tilde{c}_3 & \tilde{a}_{31} & \tilde{a}_{32} & \gamma \\
 \hline
 \mathcal{A} & b_1 & b_2 & b_3 & \tilde{\mathcal{A}} & b_1 & b_2 & b_3
 \end{array} \tag{2}$$

Observe the structural properties of this scheme: the weight vector b is the same for both schemes, and the implicit scheme is a Singly Diagonally Implicit Runge–Kutta method (SDIRK). The first property implies that there are no extra coupling order conditions for the IMEX RK scheme; that is, if both schemes have second order, the IMEX RK scheme also has second order [25]. Another advantage of IMEX RK schemes with the same weight vector b is that they preserve linear invariants of the ODE [16]. The SDIRK property is interesting from the computational point of view because it allows to solve, stage to stage, the nonlinear systems that arise when implicit RK methods are used. Actually, the Jacobian matrix may even be frozen throughout the iterations for all the stages (see [8]). Second order convergence for the IMEX RK scheme (2) leaves a total of seven degrees of freedom for optimization as we will explain later on.

The rest of the paper is organized as follows. In Section 2, we review some known results and we introduce the notation that is used throughout the paper. The coefficients of the methods as well as their properties are given in Section 3. First, in Section 3.1, we give a second order 3-stage IMEX RK method with all the properties pointed out in the introduction, amongst them, a nontrivial intersection of the stability region of the explicit RK method and the imaginary axis. It turns out that this property of the explicit scheme leads to an important decrease of the stability interval, the interval of non negativity of the stability function, and the Kraaijevanger’s coefficient. For this reason, in Section 3.2 we construct IMEX RK methods whose explicit scheme is the optimal second order 3-stage SSP RK method. In order to test the constructed schemes, some numerical experiments are given in Section 4. Some conclusions are given in Section 5. The construction process of the new IMEX schemes in this paper is given in Section 6. In Section 7 we give the coefficients and properties of some methods from the literature used in the numerical experiments.

2. Review of some known concepts

In this section we briefly review some known concepts and we introduce the notation that will be used along the paper.

2.1. Order of convergence

As we have pointed out in the introduction, the IMEX RK scheme should achieve second order. To fulfill this requirement, the following conditions should be imposed (see, for example, [25]),

$$b^t e = 1, \quad b^t c = \frac{1}{2}, \quad b^t \tilde{c} = \frac{1}{2}, \tag{3}$$

where, as usual, $e = (1, \dots, 1)^t \in \mathbb{R}$, $b = (b_1, \dots, b_s)^t$, $c = (c_1, \dots, c_s)^t$ and $\tilde{c} = (\tilde{c}_1, \dots, \tilde{c}_s)^t$; furthermore, we will also assume that

$$\mathcal{A} e = c, \quad \tilde{\mathcal{A}} e = \tilde{c}. \tag{4}$$

It is important to stress that problem parameters may affect the magnitude of the global error. This is the case for problems of the form

$$y' = F(y) + \frac{1}{\varepsilon} G(y), \tag{5}$$

where $\varepsilon \ll 1$. Uniform convergence of IMEX RK methods $(\mathcal{A}, \tilde{\mathcal{A}}, b^t, \tilde{b}^t)$ for systems of the form (5) is studied in [1]. To obtain the results, in [1], the additive ODE (5) is transformed into a partitioned system of the form

$$y' = f(y, z), \quad \varepsilon z' = g(y, z).$$

It turns out that, if

$$\tilde{b}^t \tilde{\mathcal{A}}^{-1} c = 1, \quad (6)$$

and some other conditions on the IMEX scheme hold, see [1, Theorem 3.1], then the global error satisfies

$$y_n - y(t_n) = \mathcal{O}(h^p) + \mathcal{O}(\varepsilon h^2), \quad z_n - z(t_n) = \mathcal{O}(h^2),$$

for $\varepsilon \leq Ch$, where h denotes the step size, p is the order of the explicit scheme; if, conversely, (6) is violated, the global error is of the form

$$y_n - y(t_n) = \mathcal{O}(h^p) + \mathcal{O}(\varepsilon h), \quad z_n - z(t_n) = \mathcal{O}(h).$$

2.2. Stability function for RK and IMEX RK methods

Given a RK method (\mathcal{A}, b^t) , the stability function $R(z)$ is defined as

$$R(z) = 1 + z b^t (I - z \mathcal{A})^{-1} e. \quad (7)$$

For the scalar test problem, $y' = \lambda y$, numerical approximations by RK method (\mathcal{A}, b^t) with step size h verify $y_{n+1} = R(\lambda h) y_n$.

For IMEX RK schemes $(\mathcal{A}, \tilde{\mathcal{A}}, b^t, \tilde{b}^t)$, the scalar test problem is $y' = \lambda y + i \mu y$. In this case, if the implicit scheme is used for λy and the explicit one for $i \mu y$, numerical approximations with step size h are given by $y_{n+1} = R(\lambda h, \mu h) y_n$, where the stability function $R(z, w)$ is defined as

$$R(z, w) = 1 + (i w b^t + z \tilde{b}^t) (I - i w \mathcal{A} - z \tilde{\mathcal{A}})^{-1} e. \quad (8)$$

2.3. Kraaijevanger's coefficient and regions of absolute monotonicity

For RK and IMEX RK methods, step size restrictions to obtain SSP or TVD properties are given, respectively, by the Kraaijevanger's coefficient and the region of absolute monotonicity. The literature collects an extensive research on SSP RK and SSP IMEX RK methods [2, 10, 11, 15, 18–20, 26, 30] (see [4, 6, 9, 27] for reviews on the topic).

An s -stage RK method (\mathcal{A}, b^t) is said to be absolutely monotonic at a given point $-r$, with $r \geq 0$, if the matrix $I + r \mathbb{A}$ is nonsingular, and

$$(I + r \mathbb{A})^{-1} \mathbb{A} \geq 0, \quad (I + r \mathbb{A})^{-1} e \geq 0, \quad (9)$$

where now $e = (1, 1, \dots, 1)^t \in \mathbb{R}^{s+1}$, matrix \mathbb{A} is defined by

$$\mathbb{A} = \begin{pmatrix} \mathcal{A} & 0 \\ b^t & 0 \end{pmatrix},$$

and the inequalities in (9) are understood component-wise. The Kraaijevanger's coefficient (or radius of absolute monotonicity) $\mathcal{R}(\mathbb{A})$ is defined by

$$\mathcal{R}(\mathbb{A}) = \sup\{r \mid r \geq 0 \text{ and } \mathbb{A} \text{ is absolutely monotonic on } [-r, 0]\}.$$

For RK methods, monotonicity can be ensured under a step size restriction of the form $\Delta t \leq \tau_0 \cdot \mathcal{R}(\mathbb{A})$, where τ_0 is the step size restriction for monotonicity when the explicit Euler method is used. For details see [19].

For additive RK methods, the interval limited by the Kraaijevanger's coefficient is extended to the region of absolute monotonicity [11, Definition 2.3] (see also [30]). An s -stage additive RK method $(\mathbb{A}, \tilde{\mathbb{A}})$ is said to be absolutely monotonic (a.m.) at a given point $(-r_1, -r_2)$ with $r_1, r_2 \geq 0$, if the matrix $I + r_1 \mathbb{A} + r_2 \tilde{\mathbb{A}}$ is nonsingular, $(I + r_1 \mathbb{A} + r_2 \tilde{\mathbb{A}})^{-1} e \geq 0$, and

$$(I + r_1 \mathbb{A} + r_2 \tilde{\mathbb{A}})^{-1} \mathbb{A} \geq 0, \quad (10)$$

$$(I + r_1 \mathbb{A} + r_2 \tilde{\mathbb{A}})^{-1} \tilde{\mathbb{A}} \geq 0. \quad (11)$$

The region of absolute monotonicity, $\mathcal{R}(\mathbb{A}, \tilde{\mathbb{A}})$, is defined by

$$\mathcal{R}(\mathbb{A}, \tilde{\mathbb{A}}) = \{ (r_1, r_2) \mid r_1 \geq 0, r_2 \geq 0 \text{ and } (\mathbb{A}, \tilde{\mathbb{A}}) \text{ is a.m. on } [-r_1, 0] \times [-r_2, 0] \}.$$

Numerical monotonicity can be ensured for the additive RK method $(\mathbb{A}, \tilde{\mathbb{A}})$ under the step size restriction $\Delta t \leq \min \{r_1 \tau_0, r_2 \tilde{\tau}_0\}$, where r_1 and r_2 are such that the point $(r_1, r_2) \in \mathcal{R}(\mathbb{A}, \tilde{\mathbb{A}})$, and $\tau_0, \tilde{\tau}_0 > 0$ are the step size restrictions for monotonicity when the explicit Euler method is used for functions F and G in (1), respectively (see [11] for details).

Consequently, in order to obtain nontrivial step size restrictions for RK and additive RK methods, we should have, respectively, $\mathcal{R}(\mathbb{A}) > 0$, and points $(r_1, r_2) \in \mathcal{R}(\mathbb{A}, \tilde{\mathbb{A}})$ with $r_1 > 0$ and $r_2 > 0$. In [11, 19], algebraic criteria for nontrivial Kraaijevanger's coefficient (or regions of absolute monotonicity) are given in terms of sign conditions of the coefficient matrix (or matrices), namely, $\mathbb{A} \geq 0$ (or $\mathbb{A} \geq 0, \tilde{\mathbb{A}} \geq 0$), and some inequalities of the incidence matrix of certain matrices. A trivial way to ensure these properties for IMEX RK schemes is to impose

$$a_{ij}, \tilde{a}_{ij} > 0 \text{ for } i > j, \quad b_j, \tilde{b}_j > 0, \quad \text{and} \quad \gamma > 0. \quad (12)$$

For this reason, for the IMEX RK schemes constructed in this paper we will assume the positivity conditions (12).

The step size restrictions for monotonicity obtained in terms of Kraaijevanger's coefficients and regions of absolute monotonicity are valid for general nonlinear problems. For linear problems, better step size restrictions can be obtained in terms of the radius of absolute monotonicity for linear problems, also known as the threshold factor. For details, see [7, 28, 29].

2.4. Amplification function for second order 3-point and fourth order 5-point spatial discretization

In order to study the stability of numerical schemes, we can study the dissipativity of time integrators in conjunction with spatial discretizations by means of Fourier analysis [17]. For the dissipativity analysis of advection–diffusion equations, it is sufficient to consider only the diffusion term since the advection term becomes negligible in the limit where the spatial discretization parameter tends to zero [31]. We thus consider the heat equation $u_t + a u_{xx} = 0$ and the second order 3-point spatial discretization

$$u_{xx}(x_j, t_n) \approx \frac{u_{j+1}^n - 2u_j^n + u_{j-1}^n}{(\Delta x)^2},$$

and the fourth order 5-point spatial discretization

$$u_{xx}(x_j, t_n) \approx \frac{-u_{j+2}^n + 16u_{j+1}^n - 30u_j^n + 16u_{j-1}^n - u_{j-2}^n}{(\Delta x)^2}.$$

These are two of the spatial discretizations actually implemented in ANTARES, a simulation code which numerically solves the equations of hydrodynamics and various generalizations thereof [21, 24].

When these spatial discretizations are used to solve the heat equation, we obtain an amplification function of the form

$$g(\mu, \theta) = R(-\mu h(\theta)), \quad (13)$$

where $R(z)$ is the stability function (7) of the RK method, $\mu \geq 0$, and $h : [-\pi, \pi] \rightarrow \mathbb{R}$, depends on the discretization considered. The function h satisfies $h(z) > 0$ for $z \in [-\pi, \pi]$, $z \neq 0$, and, due to the consistency of the spatial discretization, it also has the property $h(0) = 0$. Observe that $R(0) = 1$ implies $g(\mu, 0) = 1$. In particular, for the second order 3-point and for the fourth order 5-point spatial discretizations we obtain, respectively, the following functions h_3 and h_5 ,

$$h_3(\theta) = -(e^{-i\theta} - 2 + e^{i\theta}) = 4 \sin^2 \left(\frac{\theta}{2} \right), \quad (14)$$

$$h_5(\theta) = -\frac{1}{12} (16 e^{-i\theta} + 16 e^{i\theta} - e^{-2i\theta} - e^{2i\theta} - 30) = \frac{2}{3} (7 - \cos(\theta)) \sin^2 \left(\frac{\theta}{2} \right). \quad (15)$$

Since the functions h in (14) and (15) are even, $h(\theta) = h(-\theta)$, we subsequently restrict the values of θ to $\theta \in [0, \pi]$.

In the dissipativity analysis we are interested in the values:

- a) μ_0 such that, for $\mu \in [0, \mu_0]$, it holds that $g(\mu, \theta) > 0$ for $\theta \in [0, \pi]$, and
- b) μ_1 such that, for $\mu \in [0, \mu_1]$, it holds that $|g(\mu, \theta)| \leq 1$ for $\theta \in [0, \pi]$.

If $\mu_i = \infty$, $i = 0, 1$, we will understand that the interval $[0, \mu_i]$ is $[0, \mu_i)$.

It turns out that, if z_0 is the first negative zero of $R(z)$, from the definition of $g(\mu, \theta)$ in (13) we obtain that $h(\theta)\mu = -z_0$, $\theta \in [0, \pi]$. The lowest value μ_0 is given by

$$\mu_0 = -\frac{z_0}{\max_{\theta \in [0, \pi]} h(\theta)}.$$

In a similar way, if z_1 is the first negative zero of $|R(z)| - 1$, we obtain that $h(\theta)\mu = -z_1$, $\theta \in [0, \pi]$. The lowest value μ_1 is given by

$$\mu_1 = -\frac{z_1}{\max_{\theta \in [0, \pi]} h(\theta)}.$$

Observe that $[z_1, 0]$ is the stability interval of the RK method, that is, the intersection of the stability region with the real axis. In particular, for the 3–points and for the 5–points discretizations, as h_i is monotonic, we get

$$\max_{\theta \in [0, \pi]} h_3(\theta) = h_3(\pi) = 4, \quad \max_{\theta \in [0, \pi]} h_5(\theta) = h_5(\pi) = \frac{16}{3}.$$

Consequently, for each RK method, in the dissipativity analysis, it is enough to compute z_0 , the first negative zero of $R(z)$, and z_1 , the first strictly negative zero of the function $|R(z)| - 1$. For each spatial discretization, the values μ_0 and μ_1 are simply scaled values of $|z_0|$ and $|z_1|$, respectively, and thus, for our purpose, the larger $|z_0|$ and $|z_1|$, the better.

3. New second order 3–stage SSP IMEX RK schemes

In this section, we give the coefficients of the second order 3 stages IMEX RK methods of the form (2) constructed in this paper and we show their properties. The detailed derivation of the coefficients can be seen in Section 6.

Depending on their properties, each scheme will be labelled with the letters ‘L’, ‘S’, ‘P’, ‘U’, ‘M’ with the following meanings:

- ‘L’: the implicit method is L –stable;
- ‘S’: the stability region for the explicit part contains an interval on the imaginary axis;
- ‘P’: the amplification factor g for the implicit method is always positive;
- ‘U’: the IMEX RK method features uniform convergence (see condition (6));
- ‘M’: the IMEX RK method has a nontrivial region of absolute monotonicity.

Furthermore, like in [25], for the IMEX RK schemes we will use the denomination $\text{SSP}k(s, \sigma, p)$, where s and σ are the number of stages of the implicit and explicit schemes, respectively, k is the order of the SSP explicit scheme, and p is the order of the IMEX RK scheme.

In Table 1, we summarize the properties of the methods constructed. For each IMEX RK method we show the values of $w \geq 0$ such that the intervals $[-iw, iw]$ and $[-w, 0]$ are contained in the region of absolute stability, the largest value of $z > 0$ such that $R(-z) > 0$, with $R(z)$ the stability function of the method. We also give \mathcal{R}_{Lin} and \mathcal{R} which denote the radius of absolute monotonicity for linear problems and the Kraaijevanger’s coefficient, respectively. Finally, we include information on the A or L stability of the implicit scheme, and whether condition (6) for uniform convergence is satisfied.

3.1. SSP IMEX RK scheme with new implicit and explicit methods

The following new IMEX RK method

$$\begin{array}{c|ccc}
 0 & 0 & 0 & 0 \\
 \frac{5}{6} & \frac{5}{6} & 0 & 0 \\
 \frac{11}{12} & \frac{11}{24} & \frac{11}{24} & 0 \\
 \hline
 \mathcal{A} & \frac{24}{55} & \frac{1}{5} & \frac{4}{11}
 \end{array}
 \quad
 \begin{array}{c|ccc}
 \frac{2}{11} & \frac{2}{11} & 0 & 0 \\
 \frac{289}{462} & \frac{205}{462} & \frac{2}{11} & 0 \\
 \frac{751}{924} & \frac{2033}{4620} & \frac{21}{110} & \frac{2}{11} \\
 \hline
 \tilde{\mathcal{A}} & \frac{24}{55} & \frac{1}{5} & \frac{4}{11}
 \end{array}
 \quad (17)$$

has all the requirements in Section 1. We remark that for this IMEX RK method both, the implicit and the explicit schemes, are new. It is a second order IMEX RK scheme such that the implicit method is L -stable. The stability functions for the explicit and implicit schemes are

$$R_{\mathbb{A}}(z) = 1 + z + \frac{z^2}{2} + \frac{5}{36}z^3, \quad R_{\tilde{\mathbb{A}}}(z) = \frac{11(13z^2 + 110z + 242)}{2(11 - 2z)^3}. \quad (18)$$

In Figure 1 (dotted contour), we show the stability regions for the explicit and the implicit schemes in (17), as well as a zoom of this region in a neighborhood of the origin; observe that for the explicit scheme, an interval of the imaginary axis is contained in the stability region.

For the explicit scheme, we obtain $R(z) \geq 0$ for $z \in [-1.81803, 0]$, and $|R(z)| \leq 1$ for $z \in [-2.84745, 0]$. Furthermore, $|R(iw)| \leq 1$ for $w \in [-1.2, 1.2]$.

For the implicit scheme, $R(z) \geq 0$ and $|R(z)| \leq 1$ for $z \leq 0$. Furthermore, $|R(iw)| \leq 1$ for $w \in \mathbb{R}$.

In Figure 2 (dotted line), we show the stability region of the IMEX RK scheme and a zoom of this region at the origin.

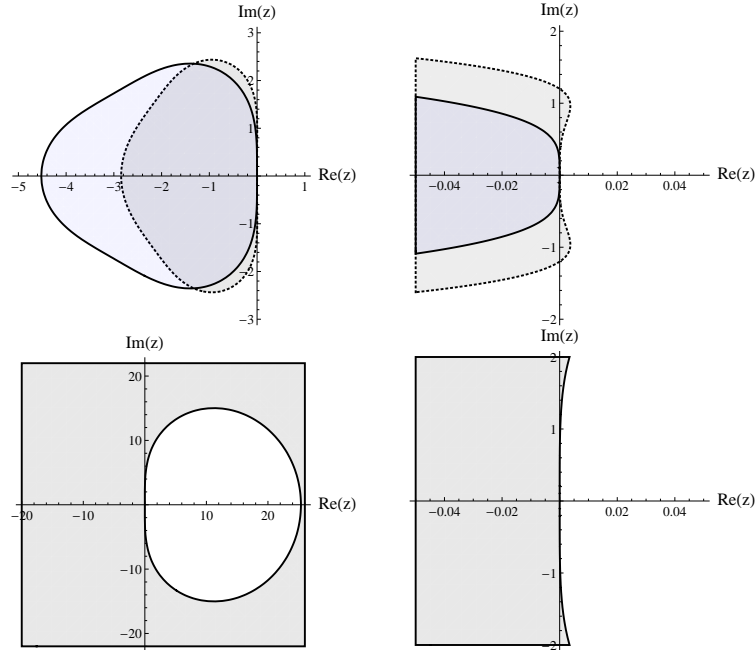


Figure 1: Top: Stability region and a zoom of this region at the origin for the explicit schemes in (17) (dotted contour), and in (20), (22) and (23) (solid contour). Bottom: Stability region and a zoom of this region at the origin for the implicit scheme in (17), (20), (22) and (23).

This IMEX RK method satisfies condition (6) for uniform convergence.

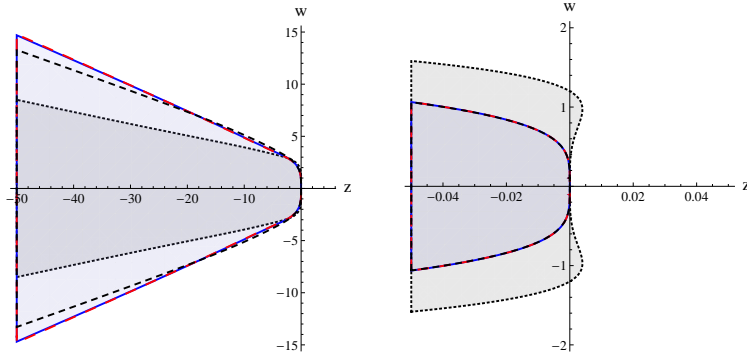


Figure 2: Stability region for the stability function (8) and a zoom of the region at the origin for the IMEX RK methods (17) (dotted line) (20) (solid line), (22) (large dashed line) and (23) (short dashed line).

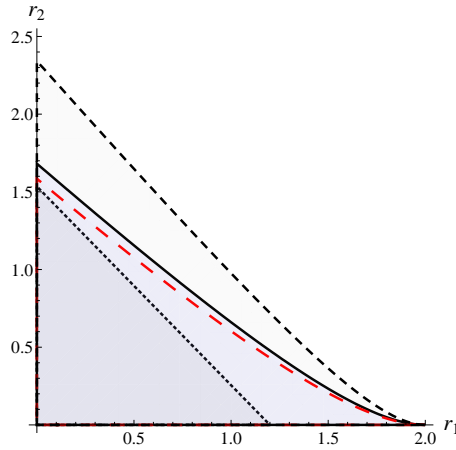


Figure 3: Regions of absolute monotonicity for the IMEX RK method (17) (dotted line) (20) (solid line), (22) (large dashed line) and (23) (short dashed line).

With regard to the radius of absolute monotonicity, for linear problems we have that

$$\mathcal{R}_{Lin}(\mathbb{A}) = 1.2, \quad \mathcal{R}_{Lin}(\tilde{\mathbb{A}}) = \frac{11}{26} \left(33 - \sqrt{517} \right) \approx 4.34177. \quad (19)$$

For nonlinear problems, we have $\mathcal{R}(\mathbb{A}) = 1.2$, $\mathcal{R}(\tilde{\mathbb{A}}) = 42/11 \approx 3.81818$, and the region of absolute monotonicity is

$$\mathcal{R}(\mathbb{A}, \tilde{\mathbb{A}}) = \left\{ (r_1, r_2) \in \mathbb{R}^2 : 0 \leq r_1 < \frac{6}{5}, 0 \leq r_2 \leq \frac{1}{43} (66 - 55 r_1) \right\}.$$

In Figure 3 (dotted contour) we show the region of absolute monotonicity for the IMEX RK method (17). The points $(0, 1.53)$ and $(1.2, 0)$ are included in the region of absolute monotonicity $\mathcal{R}(\mathbb{A}, \tilde{\mathbb{A}})$.

Due to the properties listed in (16), we will refer to scheme (17) as SSP2(3,3,2)–LSPUM. For a summary of the properties of this method, see Table 1.

3.2. IMEX RK methods with second order 3-stage optimum SSP explicit RK scheme as explicit method

In the previous section we have given a new second order 3-stage IMEX RK method with all the properties pointed out in the introduction, amongst them, a nontrivial intersection of the stability region of

Method		$[-iw, iw]$	$[-w, 0]$	$R(-z) \geq 0$	\mathcal{R}_{Lin}	\mathcal{R}	A/L -stable	(6)
(17) New/New LSPUM	Exp.	$w = 1.2$	$w = 2.85$	$z = 1.82$	1.2	1.2		Yes
	Imp.	$w = \infty$	$w = \infty$	$z = \infty$	4.34	3.82	L -stable	
(20) Opt/New LPUM	Exp.	$w = 0$	$w = 4.52$	$z = 3.59$	2	2		Yes
	Imp.	$w = \infty$	$w = \infty$	$z = \infty$	4.34	3.09	L -stable	
(22) Opt/New LPM ₍₁₎	Exp.	$w = 0$	$w = 4.52$	$z = 3.59$	2	2		No
	Imp.	$w = \infty$	$w = \infty$	$z = \infty$	4.34	3.85	L -stable	
(23) Opt/New LPM ₍₂₎	Exp.	$w = 0$	$w = 4.52$	$z = 3.59$	2	2		No
	Imp.	$w = \infty$	$w = \infty$	$z = \infty$	4.34	2.34	L -stable	

Table 1: Properties of the new IMEX RK SSP2(3,3,2) methods (17), (20), (22), (23); ‘New/New’ means that both, the implicit and the explicit schemes are new; ‘Opt/New’ means that the explicit method is the optimal SSP method and the implicit one is new. The last column denotes whether the uniform convergence condition (6) is fulfilled.

the explicit RK method with the imaginary axis. It turns out that this property for the explicit scheme leads to an important decrease of the stability interval, the interval of non negativity of the stability function, and the Kraaijevanger’s coefficient (see Table 1).

It has been argued that, in the presence of hyperbolic terms, the stability region should contain a large part of the imaginary axis even though the essentially non-oscillatory methods used for the spatial discretization have eigenvalues with a negative real part. Thus, we reconsider this property and, in this section, we give a number of additional SSP IMEX RK methods based on the optimal explicit 3-stage second order RK method in conjunction with a compatible implicit scheme. In Figure 1 (top, solid contour) we show the stability region for this explicit scheme; observe its intersection with the imaginary axis is trivial. The numerical experiments done in Section 4 will demonstrate us the convenience of this choice.

For the implicit schemes considered in this section, after imposing L -stability, non negativity of the stability function $R(z)$ for all $z \leq 0$, and second order conditions, there is one free parameter left (see Section 6.2). Hence, we construct three schemes by choosing this free parameter as follows:

1. In the first one, we impose condition (6) for uniform convergence (see Sections 3.2.1 and 6.2.1).
2. In the second one, we optimize the Kraaijevanger’s coefficient of the SDIRK scheme (see Sections 3.2.2 and 6.2.2).
3. In the third one, we optimize the region of absolute monotonicity of the IMEX RK scheme (see Sections 3.2.3 and 6.2.3).

We thus obtain schemes (20), (22) and (23). In the next sections we give their coefficients and properties.

3.2.1. IMEX RK method with uniform convergence

In this case, the IMEX RK scheme obtained by imposing condition (6) for uniform convergence is given by the coefficient tableaux

$$\begin{array}{c|ccc}
0 & 0 & 0 & 0 \\
\frac{1}{2} & \frac{1}{2} & 0 & 0 \\
1 & \frac{1}{2} & \frac{1}{2} & 0 \\
\hline
\mathcal{A} & \frac{1}{3} & \frac{1}{3} & \frac{1}{3}
\end{array}
\quad
\begin{array}{c|ccc}
\frac{2}{11} & \frac{2}{11} & 0 & 0 \\
\frac{69}{154} & \frac{41}{154} & \frac{2}{11} & 0 \\
\frac{67}{77} & \frac{289}{847} & \frac{42}{121} & \frac{2}{11} \\
\hline
\tilde{\mathcal{A}} & \frac{1}{3} & \frac{1}{3} & \frac{1}{3}
\end{array}
\tag{20}$$

The stability function for the explicit scheme is

$$R_{\mathbb{A}}(z) = 1 + z + \frac{1}{2}z^2 + \frac{1}{12}z^3, \tag{21}$$

whereas for the implicit scheme it is given by $R_{\tilde{\mathbb{A}}}(z)$ in (18), since it depends only on the diagonal element 2/11. In Figure 1 (solid contour) we show the stability regions for the explicit and the implicit methods in (20).

For linear problems, the radius of absolute monotonicity for the explicit scheme is $\mathcal{R}_{Lin}(\mathbb{A}) = 2$, whereas for the implicit scheme $\mathcal{R}_{Lin}(\tilde{\mathbb{A}})$ is given by (19). For nonlinear problems, the explicit scheme is the optimal second order 3-stage explicit SSP method and thus $\mathcal{R}(\mathbb{A}) = 2$; for the implicit method, from (9), we get

$$\mathcal{R}(\tilde{\mathbb{A}}) = \frac{1694}{275 + \sqrt{74701}} \approx 3.08947.$$

For the IMEX RK scheme, the region of absolute monotonicity is

$$\mathcal{R}(\mathbb{A}, \tilde{\mathbb{A}}) = \{(r_1, r_2) \in \mathbb{R}^2 : 0 \leq r_1 < \varphi(r_1)\},$$

with $\varphi(r_1) = (308 - 117r_1 - \sqrt{37}\sqrt{213r_1^2 - 1320r_1 + 1936})/24$. In Figures 2 and 3 (solid line) we show the stability region and the region of absolute monotonicity of the IMEX RK scheme, respectively. The points $(0, 1.68)$ and $(2, 0)$ are included in the region of absolute monotonicity $\mathcal{R}(\mathbb{A}, \tilde{\mathbb{A}})$.

Due to its properties, we will henceforth refer to method (20) as SSP2(3,3,2)-LPUM (see (16)). For a summary of the properties of this method, see Table 1.

3.2.2. IMEX RK scheme with large Kraaijevanger's coefficient $\mathcal{R}(\tilde{\mathbb{A}})$

For constructing this scheme, the free parameter is computed to obtain the largest value of $\mathcal{R}(\tilde{\mathbb{A}})$. The IMEX RK scheme obtained is

$$\begin{array}{c|ccc|ccc} 0 & 0 & 0 & 0 & \frac{2}{11} & \frac{2}{11} & 0 & 0 \\ \frac{1}{2} & \frac{1}{2} & 0 & 0 & \frac{4523}{9317} & \frac{2829}{9317} & \frac{2}{11} & 0 \\ 1 & \frac{1}{2} & \frac{1}{2} & 0 & \frac{15517}{18634} & \frac{148529}{428582} & \frac{7}{23} & \frac{2}{11} \\ \mathcal{A} & \frac{1}{3} & \frac{1}{3} & \frac{1}{3} & \tilde{\mathcal{A}} & \frac{1}{3} & \frac{1}{3} & \frac{1}{3} \end{array} \quad (22)$$

We remark that this method does not satisfy condition (6) for uniform convergence. The stability functions for the explicit and implicit RK methods in (22) are given by (21) and (18), respectively. In Figure 1 (solid contour) we show the stability regions for the explicit and the implicit methods in (22).

For linear problems, the radius of absolute monotonicity for the explicit scheme is $\mathcal{R}_{Lin}(\mathbb{A}) = 2$, whereas for the implicit scheme $\mathcal{R}_{Lin}(\tilde{\mathbb{A}})$ is given by (19). For nonlinear problems, the explicit scheme is the optimal second order 3-stage explicit SSP method and thus $\mathcal{R}(\mathbb{A}) = 2$; for the implicit method, we have

$$\mathcal{R}(\tilde{\mathbb{A}}) = \frac{11(5353 - \sqrt{18761649})}{2920} \approx 3.84822.$$

For the IMEX RK scheme, the region of absolute monotonicity is

$$\mathcal{R}(\mathbb{A}, \tilde{\mathbb{A}}) = \{(r_1, r_2) \in \mathbb{R}^2 : 0 \leq r_1 < \varphi(r_1)\},$$

where $\varphi(r_1) = 11(644 - 223r_1 - 3\sqrt{11}\sqrt{467r_1^2 - 2760r_1 + 4048})/76$. In Figures 2 and 3 (large dashed line) we show the stability region and the region of absolute monotonicity for the IMEX RK scheme, respectively. The points $(0, 1.58)$ and $(2, 0)$ are included in the region of absolute monotonicity $\mathcal{R}(\mathbb{A}, \tilde{\mathbb{A}})$.

Due to its properties, we will henceforth refer to method (22) as SSP2(3,3,2)-LPM₍₁₎ (see (16)). For a summary of the properties of this method, see Table 1.

3.2.3. IMEX RK scheme with large region of absolute monotonicity

In this case, we fix the free parameter to obtain the largest value of r_2 such that $(0, r_2) \in \mathcal{R}(\mathbb{A}, \tilde{\mathbb{A}})$. We thus obtain the IMEX RK scheme

$$\begin{array}{c|ccc|ccc} 0 & 0 & 0 & 0 & \frac{2}{11} & \frac{2}{11} & 0 & 0 \\ \frac{1}{2} & \frac{1}{2} & 0 & 0 & \frac{5003}{13310} & \frac{2583}{13310} & \frac{2}{11} & 0 \\ 1 & \frac{1}{2} & \frac{1}{2} & 0 & \frac{6271}{6655} & \frac{39731}{139755} & \frac{10}{21} & \frac{2}{11} \\ \mathcal{A} & \frac{1}{3} & \frac{1}{3} & \frac{1}{3} & \tilde{\mathcal{A}} & \frac{1}{3} & \frac{1}{3} & \frac{1}{3} \end{array} \quad (23)$$

We remark that this method does not satisfy condition (6) for uniform convergence. The stability functions for the explicit and implicit RK methods in (23) are given by (21) and (18), respectively. In Figure 1 (solid contour) we show the stability regions for the explicit and the implicit methods in (23). In Figure 2 (short dashed line) we show the stability region for the IMEX RK scheme.

For the implicit scheme,

$$\mathcal{R}(\tilde{\mathbb{A}}) = \frac{11(\sqrt{9242421} - 2641)}{1874} \approx 2.34284.$$

For the IMEX RK scheme, the region of absolute monotonicity is shown in Figure 3 (short dashed line). The points $(0, 2.34)$ and $(2, 0)$ are included in the region of absolute monotonicity $\mathcal{R}(\mathbb{A}, \tilde{\mathbb{A}})$.

We will later refer to this scheme as SSP2(3,3,2)–LPM₍₂₎ (see (16)). For a summary of the properties of this method, see Table 1.

4. Numerical experiments

In this section we study the performance of the new methods constructed in this paper named SSP2(3,3,2)–LSPUM, SSP2(3,3,2)–LPUM, SSP2(3,3,2)–LPM₍₁₎ and SSP2(3,3,2)–LPM₍₂₎, whose coefficients are given by (17), (20), (22) and (23), respectively. For the meaning of the notation L–S–P–U–M, we refer to (16).

To demonstrate the merits of the methods constructed in this paper, we also give results for some methods from the literature. More precisely, we consider the first order methods named IMEX SSP1(1,1,1)–LPM (56) and ARS(1,1,1)–LPUM (57), which are a combination of forward and backward Euler methods, and several second order methods, namely the SSP2(2,2,2)–PM scheme (58) with $\gamma = 0.24$, the SSP2(2,2,2)–LM method (58) with $\gamma = 1 - 1/\sqrt{2}$, the SSP2(2,2,2)–UM scheme (59), and the SSP2(3,3,2)–LUM method (60). A brief summary of their properties is given in Table 6.

4.1. Population model

We consider the evolution of a population density P according to the model (see [14])

$$\frac{\partial P(t, x)}{\partial t} = f(t, x) + b(x, P(t, x)) - r_d P(t, x) + d \frac{\partial^2 P(t, x)}{\partial x^2}, \quad (24)$$

where $x \in [0, 1]$ and $t \geq 0$. We assume periodic boundary conditions and zero initial condition, $P(0, t) = 0$, $x \in [0, 1]$. The birth rate $b(x, P)$ is given by

$$b(x, P) = r_b(x) \frac{\varepsilon}{\varepsilon + P}, \quad \varepsilon = 0.005,$$

where

$$r_b(x) = \begin{cases} 1, & \text{if } x \in [0, 1/2], \\ 100, & \text{if } x \in (1/2, 1]. \end{cases}$$

The death rate is set to one, i.e., $r_d = 1$, and the forcing term will be described below. In order to discretize (24), a spatial grid $\Delta x = 1/100$ is taken, and second order centered differences are used to discretize the diffusion term. The function $f(t, x)$ is taken to be zero for all times $t \neq 0$, and for each grid point $x_i = i \Delta x$, $f(0, x_i)$ is a random value in the interval $[0.8, 1.2]$. For the time stepping, the stiff diffusion term is integrated implicitly and the other terms are integrated explicitly. In the numerical experiments we consider the model with diffusion ($d = 0.02$, $d = 0.04$) and without diffusion ($d = 0$).

For this problem, the analytical solution is nonnegative for all times $t \geq 0$. In our numerical experiments we analyze the positivity preservation properties of the different IMEX RK schemes considered in this paper. For this purpose, we have computed the positivity coefficient, that is, the largest step size such that the numerical solution and the internal stages are nonnegative when the problem is integrated from $t_0 = 0$ to $t_{end} = 10$. The results are shown in Table 2. In this Table, $\mathcal{R}(\mathbb{A})$ denotes the Kraaijevanger's coefficient for the explicit scheme.

Method	order	$\mathcal{R}(\mathbb{A})$	$\Delta t(d=0)$	$\Delta t(d=0.02)$	$\Delta t(d=0.04)$
(17) SSP2(3,3,2)–LSPUM	2	1.2	1.204	1.203	1.240
(20) SSP2(3,3,2)–LPUM	2	2	2.008	1.275	1.461
(22) SSP2(3,3,2)–LPM ₍₁₎	2	2	2.008	2.049	2.127
(23) SSP2(3,3,2)–LPM ₍₂₎	2	2	2.008	0.488	0.507
(56) SSP1(1,1,1)–LPM	1	1	1.004	1.004	1.004
(57) ARS(1,1,1)–LPUM	1	1	1.004	1.092	1.144
(58) SSP2(2,2,2)–LM $\gamma = 1 - 1/\sqrt{2}$	2	1	1.004	0.444	0.452
(59) SSP2(2,2,2)–UM	2	1	1.004	0.660	0.786
(60) SSP2(3,3,2)–LUM	2	2	2.008	1.482	1.615

Table 2: Largest step size for non negativity. Top: new second order methods ((17), (20), (22) and (23)). Center: first order methods from the literature ((56) and (57)). Bottom: second order methods from the literature ((58), (59) and (60)).

It can be seen that, for the first order methods (56) and (57), the positivity coefficient does not change significantly when d is modified. A similar situation holds for the new second order schemes (17) and (22). For the rest of the methods, the positivity coefficient for $d = 0.02$ and $d = 0.04$ is smaller than the one for $d = 0$. However, the new method (20) and the scheme (60) have $\mathcal{R}(\mathbb{A}) = 2$ and, although the positivity coefficient is decreased when d is increased, the positivity coefficient for $d = 0.04$ is larger than the one obtained with some IMEX RK schemes that preserve it, namely methods (17), (56) and (57).

From the results obtained in this positivity test, the best second order IMEX RK schemes are (17), (20), (22), and (60). Poor results are obtained with the IMEX RK methods (23) and (58) with $\gamma = 1 - 1/\sqrt{2}$.

In order to check the quality of the numerical solutions, we have computed the numerical solution at $t_{end} = 10$ with step size $\Delta t = 0.25$. For all the methods, this step size ensures positivity of the numerical solution, however, the qualitative properties of the solution are not always correct. At $t_{end} = 10$, the exact solution has a positive smooth profile.

In Figure 4 we show the results for schemes SSP1(1,1,1)–LPM method (56), SSP2(3,3,3)–LPM₍₁₎ method (22) and SSP2(3,3,3)–LPM₍₂₎ method (23). It can be seen that the solution is not smooth in a neighborhood of $x = 0.5$.

The numerical solution for methods SSP2(3,3,2)–LSPUM (17), SSP2(3,3,2)–LPUM (20) and SSP2(3,3,2)–LUM (60) is given in Figure 5. Observe that for these methods, the numerical solution is smooth. Observe too that all these methods have the ‘U’ property.

Finally, in Figure 6 we show the results for methods ARS(1,1,1)–LPUM (57), SSP2(2,2,2)–UM (59) and SSP2(2,2,2)–LM method (58) with $\gamma = 1 - 1/\sqrt{2}$. Observe that for ARS(1,1,1)–LPUM (57) and SSP2(2,2,2)–UM (59) schemes, the solution is smooth, but a nonsmooth profile is obtained when SSP2(2,2,2)–LM method (58) with $\gamma = 1 - 1/\sqrt{2}$ is used. However, ARS(1,1,1)–LPUM method (57) is a first order method, and the implicit method in SSP2(2,2,2)–UM scheme (59) is not L -stable. Hence, they are not appropriate methods for the models in astrophysics were are interested in.

Summarizing up, the numerical experiments done for the population model (24) show that the most robust second order schemes are the ones named SSP2(3,3,2)–LSPUM (17), SSP2(3,3,2)–LPUM (20) and SSP2(3,3,2)–LUM (60). All them have the ‘LU’ property. Schemes lacking the ‘U’ property yield unacceptable accuracy near $x = 0.5$ (and $x = 0$) for the test problem.

4.2. Linear advection–reaction

We consider now the linear constant coefficient problem [14]

$$\begin{aligned} u_t + \alpha_1 u_x &= -k_1 u + k_2 v + s_1, \\ v_t + \alpha_2 v_x &= k_1 u - k_2 v + s_2, \end{aligned}$$

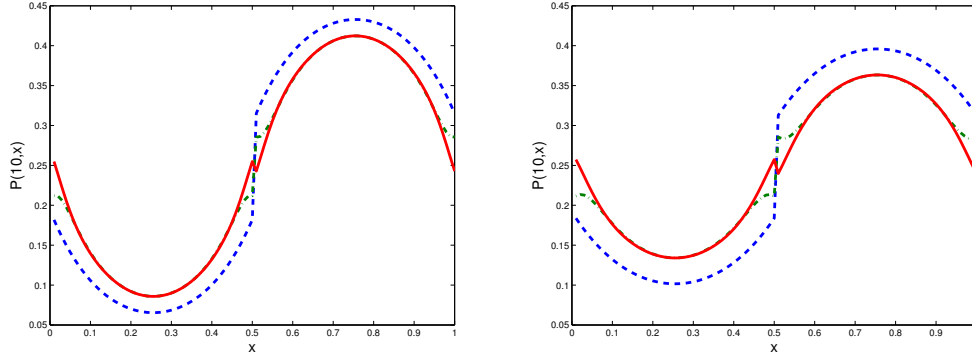


Figure 4: Numerical solution at $t_{end} = 10$ with step size $\Delta t = 0.25$. Dashed line: SSP1(1,1,1)-LPM method (56); solid line: SSP2(3,3,2)-LPM₍₁₎ method (22); dashed dotted line: SSP2(3,3,2)-LPM₍₂₎ method (23). Left: $d = 0.02$. Right: $d = 0.04$.

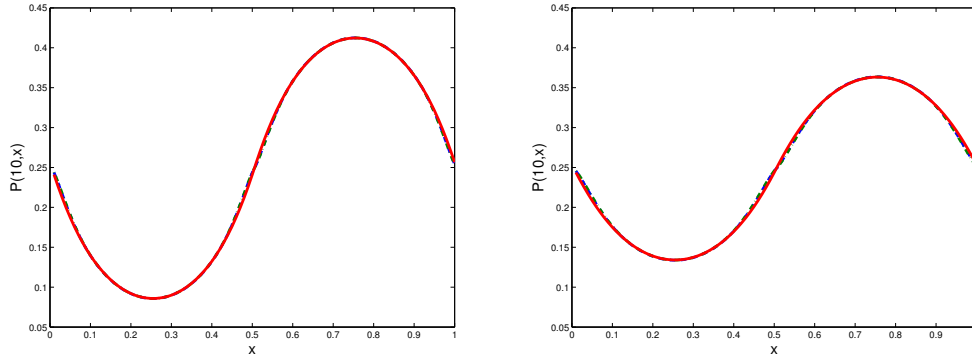


Figure 5: Numerical solution at $t_{end} = 10$ with step size $\Delta t = 0.25$. Dashed line: SSP2(3,3,2)-LSPUM method (17); dashed dotted line: SSP2(3,3,2)-LPUM method (20); solid line: SSP2(3,3,2)-LUM scheme (60). Left: $d = 0.02$. Right: $d = 0.04$.

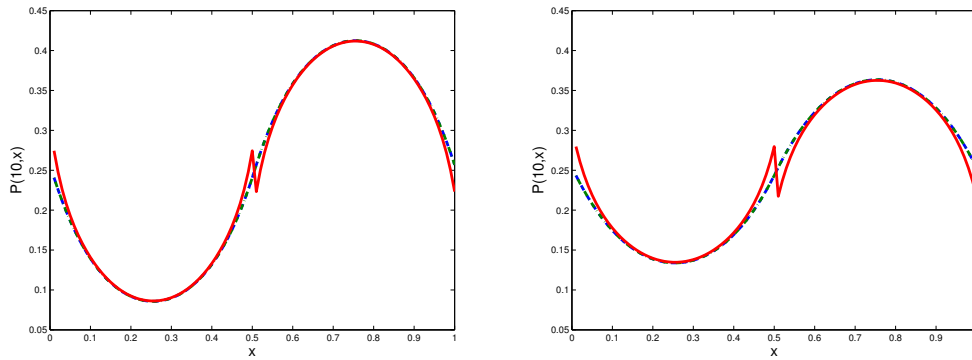


Figure 6: Numerical solution at $t_{end} = 10$ with step size $\Delta t = 0.25$. Dashed line: ARS(1,1,1)-LPUM method (57); dashed dotted line: SSP2(2,2,2)-UM method (59); solid line: SSP2(2,2,2)-LM with $\gamma = 1 - 1/\sqrt{2}$ method (58). Left: $d = 0.02$. Right: $d = 0.04$.

for $0 < x < 1$, $0 < t < 1$, where $\alpha_1 = 1$, $\alpha_2 = 0$, $k_1 = 10^6$, $k_2 = 2k_1$, $s_1 = 0$ and $s_2 = 1$. The initial and boundary values are

$$u(x, 0) = 1 + s_2 x, \quad v(x, 0) = \frac{k_1}{k_2} u(x, 0) + \frac{1}{k_2} s_2, \quad u(0, y) = \gamma_1(t).$$

In our tests, we consider a uniform spatial grid, $x_i = i \Delta x$, $i = 1, \dots, m$, with $\Delta x = 1/m$. The errors are measured at the final time $t = 1$ in the L_1 -norm (for $v \in \mathbb{R}^M$, $\|v\|_1 = \sum_i |v_i|/M$).

Like in [14], we consider $\gamma = 1$. In this case, the initial values provide a stationary solution. We consider first order upwind spatial discretization with $m = 100$. In Table 3 we show the L_1 errors for the v -component at time $t = 1$ for different step sizes.

The best results are obtained for the first order method ARS1(1,1,1)–LPUM (57) and the second order scheme SSP2(2,2,2)–UM (59); these methods are internally consistent, that is, $c = \tilde{c}$. The next best results are obtained for methods SSP2(3,3,2)–LSPUM (17), SSP2(3,3,2)–LPUM (20) and SSP2(3,3,2)–LUM (60); observe that these methods are not internally consistent but all them have the ‘U’ property. Finally, poor results are obtained for schemes SSP1(1,1,1)–LPM (56), SSP2(3,3,2)–LPM₍₁₎ (22), SSP2(3,3,2)–LPM₍₂₎ (23) and SSP2(2,2,2)–LM (58) with $\gamma = 1 - 1/\sqrt{2}$; these schemes are not internally consistent and none of them has the ‘U’ property.

We can conclude that, for this problem, internal consistency of IMEX RK method is an important property for accuracy and, for non internally consistent IMEX RK methods, the ‘U’ property improves the performance of the method (by 3 or 4 orders of magnitude for the test case, as demonstrated by the results given in Table 3).

Method	Δt	1.00×10^{-2}	5.00×10^{-3}	2.50×10^{-3}	1.25×10^{-3}
(17) SSP2(3,3,2)–LSPUM		9.2391e-06	2.2271e-06	9.2146e-07	6.4179e-07
(20) SSP2(3,3,2)–LPUM		5.5986e-06	1.5010e-06	7.6739e-07	6.0671e-07
(22) SSP2(3,3,2)–LPM ₍₁₎		7.2003e-04	3.6005e-04	1.8023e-04	9.0357e-05
(23) SSP2(3,3,2)–LPM ₍₂₎		2.1734e-03	1.0851e-03	5.4191e-04	2.7052e-04
(56) SSP1(1,1,1)–LPM		1.1333e-03	5.6111e-04	2.7917e-04	1.3924e-04
(57) ARS(1,1,1)–LPUM		1.6188e-12	1.1466e-12	2.0449e-13	1.2392e-13
(58) SSP2(2,2,2)–LM $\gamma = 1 - 1/\sqrt{2}$		2.3672e-03	1.1804e-03	5.8904e-04	2.9389e-04
(59) SSP2(2,2,2)–UM		1.8649e-12	1.0865e-12	7.0969e-13	3.6493e-13
(60) SSP2(3,3,2)–LUM		2.3335e-06	5.0145e-07	1.5501e-07	7.8302e-08

Table 3: Stationary solution, $m = 100$, L_1 -errors versus step size. Top: new second order methods ((17), (20), (22) and (23)). Center: first order methods from the literature ((56) and (57)). Bottom: second order methods from the literature ((58), (59) and (60)).

4.3. Simulation of double-diffusive convection

To demonstrate the capabilities and limitations of the time integrators discussed in the previous sections, we tested the methods on simulations of double-diffusive convection. Double-diffusive convection is a phenomenon encountered for example in stellar interiors. Models of stellar structure and evolution predict a setting where the heavier products of nuclear fusion provide stability to a zone which otherwise would be unstable to convective overturning since temperature increases sufficiently rapidly against the direction of gravity. The question whether such a zone should be treated as if it were mixed or not has become known as the *semiconvection problem*. In the present context, simulations of double-diffusive convection in an idealized setting are performed with the hydrodynamics code ANTARES [24]. The model equations are the compressible two-component Navier-Stokes equations. The initial setting consists of a hydrostatically stable but thermally unstable configuration. To start dynamics away from equilibrium, a random initial

perturbation is applied. For a detailed description of the model, the reader is referred to [21]; details on the semiconvection problem are found in [34].

The challenge of these simulations is that they require the time integration method to work for quite different conditions within a single simulation run: only a method which can handle stiff terms and is also SSP can succeed with acceptable time-steps. The equations to be solved are of the form

$$\underbrace{\frac{d}{dt} \begin{pmatrix} \rho \\ \rho c \\ \rho \mathbf{u} \\ e \end{pmatrix}}_{y'(t)} = -\nabla \cdot \underbrace{\begin{pmatrix} \rho \mathbf{u} \\ \rho c \mathbf{u} \\ \rho \mathbf{u} \otimes \mathbf{u} + P - \sigma \\ e \mathbf{u} + P \mathbf{u} - \mathbf{u} \cdot \sigma \end{pmatrix}}_{F(y(t))} - \underbrace{\begin{pmatrix} 0 \\ 0 \\ \rho g \\ \rho g \mathbf{u} \end{pmatrix}}_{G(y(t))} + \nabla \cdot \underbrace{\begin{pmatrix} 0 \\ \rho \kappa_c \nabla c \\ 0 \\ K \nabla T \end{pmatrix}}_{G(y(t))}. \quad (25)$$

The basic fields ρ , c , \mathbf{u} , and e all directly depend on the time coordinate t and spatial coordinates (two in the example given below) while the other functions directly depend on ρ , c , and e ; g is a constant function in that example and σ is an analytical function with similar dependencies as the term $\rho \kappa_c \nabla c$.

The setting chosen for this paper is similar to *Simulation 1* in [21], namely, we assume a Prandtl number $Pr = 0.05$ (instead of 0.1), a Lewis number $Le = 0.05$ (instead of 0.1), a modified Rayleigh number $Ra^* = Ra \cdot Pr = 1.6 \cdot 10^5$, and a stability parameter $R_\rho = 1.15$ (instead of 1.1). These dimensionless numbers measure the size of the terms in (25) relative to each other by comparing diffusivities (or conductivities) such as κ_c and K , the viscosity (contained in σ), and the driving through boundary conditions and local gravitational acceleration. In the astrophysical case, $Le < Pr < 1$ while $Ra^* \gg 1$ and R_ρ is frequently of order unity. The nature of the flow sensitively depends on the value of R_ρ (cf. Fig. 3 in [34]). In comparison with giant planets [22], for stars it holds in addition that $Pr \ll 1$ [33]. By comparison, for the salt water as it occurs in the oceans on Earth, $Pr \sim 7$ and $Le < 1 < Pr$. For this scenario, one important problem from a numerical point of view is that the time step may be limited by the diffusivities even though the time evolution of the solution only occurs on the much longer hydrodynamical (or flow) timescale. In some cases, as in the example shown below, even a transition between the diffusion dominated and the advection dominated regime can occur. This challenges schemes proposed for the time integration of this kind of problems.

In the following, we test the schemes named SSP2(3,3,2)–LSPUM, SSP2(3,3,2)–LPUM, and SSP2(3,3,2)–LPM₍₂₎, whose coefficients are given by (17), (20), and (23), respectively. We do not consider schemes SSP2(2,2,2)–UM (59) and SSP2(3,3,2)–LPM₍₁₎ (22) because (59) is not L –stable and (22) has properties similar to (23) and a smaller region of absolute monotonicity. For the meaning of the notation L–S–P–U–M, we refer to (16). For spatial resolution, 429×428 grid points were used. Simulation time is measured in units of *sound crossing times* (sct). The simulations were run on the *Vienna Scientific Cluster (VSC) 1* on 64 CPUs.

To demonstrate the merits of the methods constructed in this paper, we also give results for the method IMEX SSP1(1,1,1)–LPM (56), which is a combination of the forward and backward Euler methods. It becomes clear that such a simple low order scheme is not advisable for our purposes. For a better comparison, we also list the best performing schemes of [21], namely the SSP2(2,2,2)–PM scheme (58) with $\gamma = 0.24$ and the SSP2(3,3,2)–LUM method (60).

According to [21], the time-step used is determined as

$$\tau_{\text{diff}} = \min(\tau_c, \tau_T), \quad \Delta t = \min(\tau_{\text{diff}}, \tau_{\text{visc}}, \tau_{\text{fluid}}).$$

In the present simulations, this criterion results in τ_{diff} posing a lower bound and τ_{visc} posing an upper limit on τ . As soon as the fluid velocity is high enough to pose a more severe restriction than τ_{visc} , the simulation migrates from the *diffusive phase* to the *advective phase* and τ_{fluid} replaces τ_{visc} as an upper limit on τ . The time-step is regulated by the adaptive time-step control of [21].

In Table 4 we show the time-steps, CFL–numbers and wallclocktimes over the first 80 sct. The CFL_{max}– and CFL_{mn}–numbers are calculated by

$$\text{CFL}_{\text{max}} = \text{CFL}_{\text{start}} \frac{\tau_{\text{max}}}{\tau_{\text{start}}}, \quad \text{CFL}_{\text{mn}} = \text{CFL}_{\text{start}} \frac{\tau_{\text{mn}}}{\tau_{\text{start}}},$$

Method	Δt_{\max}	Δt_{mean}	CFL_{\max}	CFL_{mean}	$\text{CFL}_{\text{start}}$	Time
SSP2(3,3,2)– LSPUM (17)	125.14 s	75.53 s	5.8	3.5	0.3	00:45:17
SSP2(3,3,2)– LPUM (20)	179.54 s	86.79 s	8.31	4.02	0.3	00:31:16
SSP2(3,3,2)– LPM ₍₂₎ (23)	58.57 s	38.51 s	2.71	1.8	0.3	00:57:23
SSP1(1,1,1)– LPM (56)	15.33 s	1.15 s	0.71	0.053	0.05	9:36:12
SSP2(2,2,2)– PM, $\gamma=0.24$ (58)	26.02 s	15.02 s	1.22	0.7	0.5	01:55:47
SSP2(3,3,2)– LUM (60)	79.60 s	48.33 s	3.7	2.24	0.4	00:51:58

Table 4: Simulation of double-diffusive convection: Time-steps, CFL-numbers and wallclocktimes over the first 80 scrt. Top: new second order methods ((17), (20) and (23)). Center: first order methods from the literature ((56) and (57)). Bottom: second order methods from the literature ((58) and (60)).

where τ_{start} denotes the (starting) timestep computed using $\text{CFL}_{\text{start}}$.

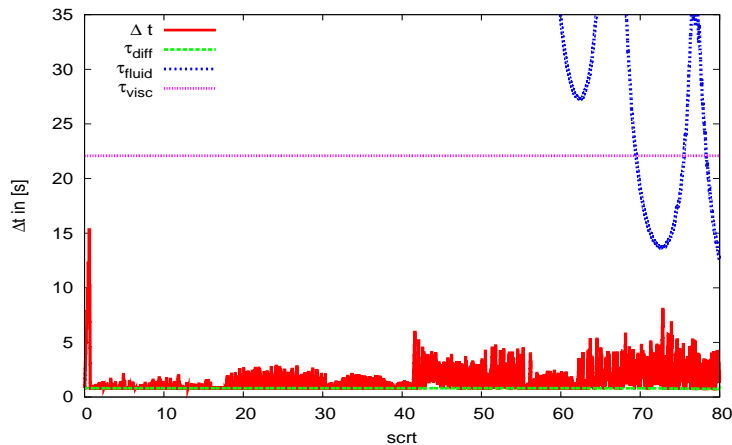


Figure 7: Simulation of double-diffusive convection: Time-step evolution with time integrator IMEX SSP1(1,1,1)–LPM (56).

For IMEX SSP1(1,1,1)–LPM (56), the time-steps observed in the course of the simulation are shown in Figure 7. Figure 8 compares the time-step evolution of the different time integration schemes whereas the Figures 9, 10, 11, and 12 show the time-step evolution of each simulation in more detail.

4.3.1. Resolution Test

Due to the fact that the upper limit set by τ_{visc} is not reached in the simulations, we perform a resolution test to determine whether this discrepancy results from the inaccuracy of the spatial discretization. To this end, the first 20 scrt are run with a resolution of 229x228, 429x428, 829x828, and 1629x1628 grid points. Table 5 compares the observed Courant numbers. Note that the Courant numbers given for the simulation with a resolution of 429x428 grid points in Table 5 differ from those given in Table 4. This is due to the fact that in Table 5 the mean and maximum CFL-numbers are taken over the first 20 scrt of the simulation whereas in Table 4 the first 80 scrt are considered. Indeed, the Courant numbers appear to display some trend as the resolution improves.

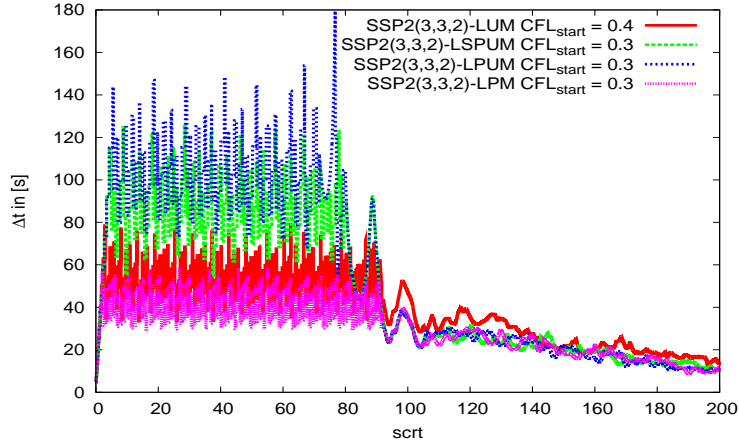


Figure 8: Simulation of double-diffusive convection: Time-step evolution over the entire 200 \sqrt{t} for schemes SSP2(3,3,2)-LUM (60), SSP2(3,3,2)-LSPUM (17), SSP2(3,3,2)-LPUM (20) and SSP2(3,3,2)-LPM₍₂₎ (23).

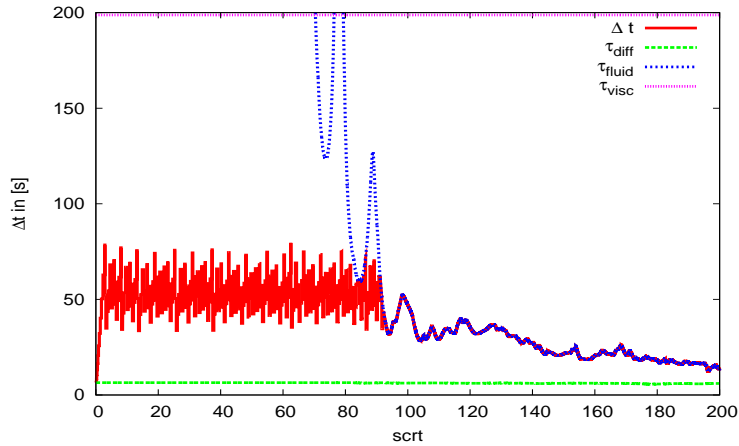


Figure 9: Simulation of double-diffusive convection: Time-step evolution with time integrator IMEX SSP2(3,3,2)-LUM (60) and $CFL_{start} = 0.4$.

4.3.2. Summary of numerical tests

The results obtained for the simulation of double-diffusive convection shows that the schemes SSP2(3,3,2)-LSPUM (17) and SSP2(3,3,2)-LPUM (20), which are constructed so as to permit the highest possible time-step in the diffusive regime, are not only competitive to the schemes of [21] but in particular enabled to reach the highest CFL numbers. Especially IMEX SSP2(3,3,2)-LPUM (20) achieves a mean CFL number of 4.02, which is about 79.5% higher than the mean CFL number of SSP2(3,3,2)-LUM (60).

The maximum time-step of IMEX SSP2(3,3,2)-LSPUM is impressive, however, a quick glance at Figure 11 show that this number results from a singular peak at the beginning of the advective phase. The mean time-steps of IMEX SSP2(3,3,2)-LPUM differ only by about 15% (86.79 s versus 75.53 s). Nevertheless, this difference already results in an increase of computational efficiency of about 40% (45 min versus 31 min). The higher time-steps achieved by IMEX SSP2(3,3,2)-LPUM also indicate that the property ‘S’, that is, the inclusion of a portion of the imaginary axis in the stability region of the explicit Runge-Kutta scheme, is of little importance in the present simulations.

It is interesting to note that, although there are almost no differences in the specifications of SSP2(3,3,2)-LPUM (20), and SSP2(3,3,2)-LPM₍₂₎ (23) as far as zeros of the stability function, radii of absolute monotonicity etc. are concerned (see Table 1), the SSP2(3,3,2)-LPM₍₂₎ scheme (23) performs considerably worse

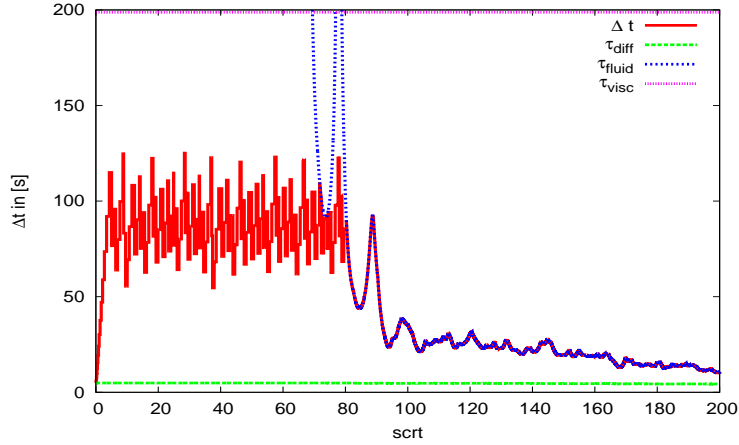


Figure 10: Simulation of double-diffusive convection: Time-step evolution with time integrator IMEX SSP2(3,3,2)-LSPUM (17) and $CFL_{start} = 0.3$.

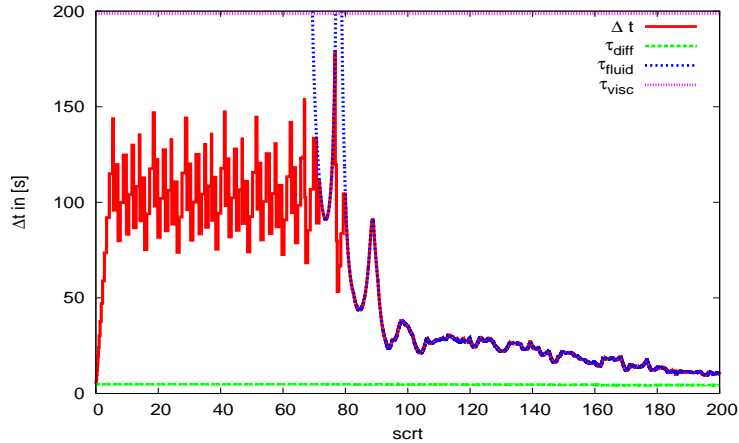


Figure 11: Simulation of double-diffusive convection: Time-step evolution with time integrator IMEX SSP2(3,3,2)-LPUM (20) and $CFL_{start} = 0.3$.

than SSP2(3,3,2)-LPUM method (20). The crucial deficiency in this context seems to be the property of uniform convergence, which SSP2(3,3,2)-LPUM (20) possesses and SSP2(3,3,2)-LPM₍₂₎ (23) lacks.

The first order IMEX SSP1(1,1,1) performs worst among all schemes which have been tested here. For a stable integration, extremely small time steps ($CFL_{start} = 0.05$!) need to be employed, rendering the simulation to be about 18.6 times slower (9h 36 min against 31 min) than the best performing IMEX SSP2(3,3,2)-LPUM scheme (20).

Our experiments show that, while the time-step in the diffusive phase is significantly larger, in the advective phase the calculation is slowed down such that there is almost no benefit from the new time integration schemes in this kind of setting as far as computation time is concerned. The new schemes would in turn be clearly favored for problems where the restriction in time stepping is mostly or exclusively due to τ_{diff} during the entire simulation time.

5. Conclusions

We have constructed and analyzed IMEX RK methods which, in addition to being SSP, have properties which increase their performance for the time integration of different kind of problems, in particular, models

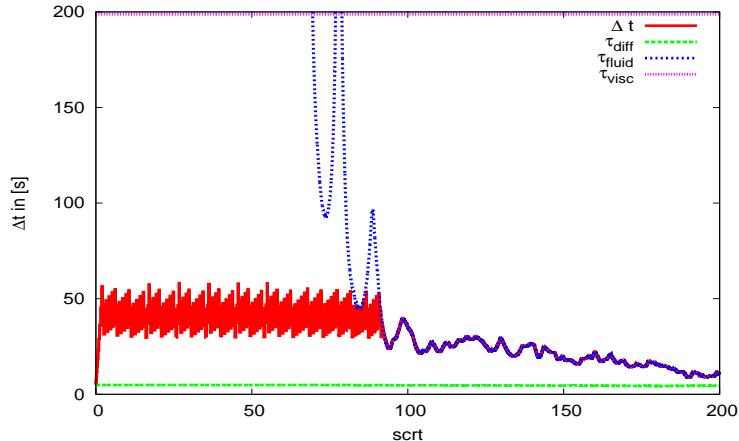


Figure 12: Simulation of double-diffusive convection: Time-step evolution with time integrator IMEX SSP2(3,3,2)-LPM₍₂₎ (23) and CFL_{start} = 0.3.

SSP2(3,3,2)-LSPUM (17)			SSP2(3,3,2)-LPUM (20)		
Resolution	CFL _{mn}	CFL _{max}	Resolution	CFL _{mn}	CFL _{max}
229x228	1.42	3.7	229x228	1.44	3.27
429x428	2.7	5.8	429x428	3.0	6.81
829x828	3.7	6.0	829x828	4.2	7.45
1629x1628	3.82	6.3	1629x1628	4.86	7.72

Table 5: Resolution test for the simulation of double-diffusive convection. Left: SSP2(3,3,2)-LSPUM method (17). Right: SSP2(3,3,2)-LPUM method (20).

of flow and radiative transfer in astrophysics. Instead of trying to optimize the methods with one stability criterium, we try to impose several stability properties. This way of proceeding allows us to obtain robust methods which are of interest for different classes of problems.

The methods are constructed to be SSP, where this property is shared by both the explicit and implicit subschemes. Moreover, the stability regions cover significant parts of the negative real axis, which also directly translates into large time-steps to allow a dissipative, non-oscillatory behavior in conjunction with suitable finite difference discretizations of the diffusion terms. With the further requirements of L -stability and positivity, this motivated the construction of three-stage second order schemes. The integration of the hyperbolic terms mandates to also have a large portion of the imaginary axis in the stability domain and, consequently, we have also taken into account this property. We combine known optimal explicit SSP or new explicit SSP schemes with compatible implicit methods and construct new pairs of schemes. Proceeding in this way, we have obtained four new IMEX RK methods.

We have tested them for a simple diffusion reaction problem with a nonnegative solution. The most robust methods are the IMEX RK methods named SSP2(3,3,2)-LSPUM (17), SSP2(3,3,2)-LPUM (20) and SSP2(3,3,2)-LUM (60). Our second test to compute the stationary solution of a linear advection reaction system also shows a good performance of these methods. These results also agree with the ones obtained in [13] in the context of Black-Scholes equation, where the use of method SSP2(3,3,2)-LSPUM (17) avoids undesirable oscillations when the greeks are computed.

We also show that this increase in performance is obtained in practice in simulations in the parameter regime commonly associated with double-diffusive or semiconvection. It turns out that the new schemes SSP2(3,3,2)-LSPUM (17) and SSP2(3,3,2)-LPUM (20) have the best properties and also show the best performance in numerical tests in different parameter regimes. Indeed, for this problem, the best known

scheme, SSP2(3,3,2)–LUM (60), requires computation times 15% and 67% higher than our newly constructed methods (17) and (20), respectively, which in turn achieve mean CFL numbers up to 56% and 79.5% higher, and maximum CFL numbers up to 56% and 124% higher than method SSP2(3,3,2)–LUM (60). Our tests shows that, although the mean time–steps of IMEX SSP2(3,3,2)–LPUM (20) and SSP2(3,3,2)–LSPUM (17) differ only about 15% (86.79 s versus 75.53 s), this difference results in an increase of computational efficiency of about 40% (45 min versus 31 min). Furthermore, the higher time–steps achieved by IMEX SSP2(3,3,2)–LPUM (20) also indicate that the property ‘S’, that is, the inclusion of a portion of the imaginary axis in the stability region of the explicit Runge-Kutta scheme, seems to be of little importance in double–diffusive convection simulations.

Due to the accumulation of different stability properties, the optimized IMEX-RK methods SSP2(3,3,2)–LSPUM (17) and SSP2(3,3,2)–LPUM (20) obtained in this paper are robust schemes that may also be useful for general problems which involve the solution of advection–diffusion equations or other transport equations with similar stability requirements.

6. Appendix A: Construction of the schemes

In this section we show in detail how the different methods are constructed. We proceed step to step, trying to impose the properties pointed out in Section 1. Due to the limited number of free parameters, sometimes it is not possible to optimize at the same time two different properties and some choices must be done. Numerical experiments have to show which properties are more relevant for the problems one is interested in. The coefficients of the methods in this section have been obtained with the help of the symbolic computation software *Mathematica*.

6.1. A new second order 3 stages SSP IMEX RK scheme

In this section we construct a new second order 3–stage SSP IMEX RK scheme of the form (2) with all the requirements explained in Section 1. We begin constructing the explicit scheme and, in a second step, we will deal with the implicit one. Finally, we will fix the remaining free parameters to obtain the desired properties for the IMEX RK scheme.

6.1.1. Explicit scheme

Condition (4) and second order conditions (3) for the explicit scheme lead to

$$b_1 = 1 - b_2 - b_3, \quad c_3 = \frac{1 - 2b_2c_2}{2b_3}, \quad a_{21} = c_2, \quad a_{31} = c_3 - a_{32}. \quad (26)$$

Hence, four degrees of freedom of the explicit scheme are left to be determined after the previous considerations. For a second order 3–stage explicit scheme, the stability function is given by [8]

$$R(z) = 1 + z + \frac{z^2}{2} + b_3 a_{32} c_2 z^3.$$

Thus, defining

$$a_{32} = \frac{\alpha}{b_3 c_2}, \quad (27)$$

we obtain the stability function

$$R(z) = 1 + z + \frac{z^2}{2} + \alpha z^3. \quad (28)$$

To express the four degrees of freedom, in the following we choose α , c_2 , b_2 , and b_3 . In the next subsection, we study the stability function (28) and the stability region \mathcal{S} in terms of α .

Stability function for the explicit scheme. We study the stability function (28) to determine the values of α such that the method fulfills all the desired requirements.

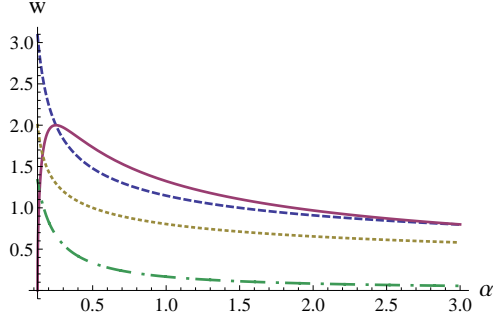


Figure 13: For $\alpha \in [1/8, 3]$. Continuous line: $w > 0$ such that $[-iw, iw] \in \mathcal{S}$; dashed line: $z > 0$ such that $[-z, 0] \in \mathcal{S}$; dotted line: $z > 0$ such that $R(-z) \geq 0$; dashed-dotted line: $\mathcal{R}_{Lin}(\mathbb{A})$.

- *Intersection of the stability region with the imaginary axis.* To obtain the intersection of the stability region \mathcal{S} with the imaginary axis, we study the values of α such that $|R(iw)| \leq 1$. In our case, from

$$R(iw) = 1 - \frac{w^2}{2} + i(w - w^3\alpha),$$

we obtain that, for $\alpha > 1/8$, the interval $[-iw(\alpha), iw(\alpha)]$ is contained in the stability region \mathcal{S} , where $w(\alpha) = \sqrt{8\alpha - 1}/(2\alpha)$. The plot for $w(\alpha)$ can be seen in Figure 13 (continuous line). The maximum value is $w(1/4) = 2$. In particular, we obtain that the interval $[-i, i]$ is contained in the stability region \mathcal{S} for

$$\alpha \in \left[\frac{1}{2} (2 - \sqrt{3}), \frac{1}{2} (2 + \sqrt{3}) \right] \approx [0.133975, 1.86603]. \quad (29)$$

- *Intersection of the stability region with the real axis.* To obtain the intersection of the stability region \mathcal{S} with the real axis, we study the values of $w > 0$ such that $|\mathcal{R}(-w)| \leq 1$. In Figure 13 (dashed line), we see the values of $w(\alpha)$ for $\alpha > 1/8$.
- *Non negativity of the stability function.* We study the points $w > 0$ such that $R(-w) \geq 0$. In Figure 13 (dotted line), we show the values of $w(\alpha)$ such that $R(z) \geq 0$ for $z \in [-w(\alpha), 0]$, when $\alpha > 1/8$.

Radius of absolute monotonicity for linear problems. In order to obtain the radius of absolute monotonicity for linear problems (or the threshold factor), we compute the Taylor expansion of the stability function (28) at $x = -r$ to obtain

$$R(z) = 1 - r + \frac{r^2}{2} - r^3\alpha + (1 - r + 3r^2\alpha)(r+z) + \left(\frac{1}{2} - 3r\alpha\right)(r+z)^2 + \alpha(r+z)^3.$$

The largest value r such that all the coefficients are nonnegative is the radius of absolute monotonicity of the method [28, 29]. For $\alpha \geq 1/8$, we observe that all the coefficients are nonnegative if $r \leq 1/(6\alpha)$, and hence the radius of absolute monotonicity for the linear problem is given by

$$\mathcal{R}_{Lin}(\mathbb{A}) = \frac{1}{6\alpha}. \quad (30)$$

In Figure 13 (dashed-dotted line) we show the radius of absolute monotonicity as a function of α . Recall that, for explicit second order 3-stage RK methods, the optimal radius of absolute monotonicity for linear problems $\mathcal{R}_{Lin}(\mathbb{A}) = 2$ is obtained for $\alpha = 1/12$ [20]. However, for $\alpha = 1/12$ there is not any interval of the imaginary axis contained in the stability region \mathcal{S} , as this requires $\alpha > 1/8$.

Kraaijevanger's coefficient. For nonlinear problems, the Kraaijevanger's coefficient $\mathcal{R}(\mathbb{A})$ satisfies $\mathcal{R}(\mathbb{A}) \leq \mathcal{R}_{Lin}(\mathbb{A})$ [19]. In our case, if

$$b_2 = \frac{1}{36\alpha}, \quad c_2 = 6\alpha, \quad \frac{1}{36\alpha} \leq b_3 \leq \frac{18\alpha - 1}{18\alpha}, \quad (31)$$

after some computations, from (9) we obtain that

$$\mathcal{R}(\mathbb{A}) = \mathcal{R}_{Lin}(\mathbb{A}) = \frac{1}{6\alpha}. \quad (32)$$

Choice of α . So far, after imposing (26)–(27) and (31), we have two free parameters left, namely b_3 and α , that should satisfy

$$\frac{1}{36\alpha} \leq b_3 \leq \frac{18\alpha - 1}{18\alpha}, \quad \alpha \in \left[\frac{1}{2}(2 - \sqrt{3}), \frac{1}{2}(2 + \sqrt{3}) \right] \approx [0.133975, 1.86603].$$

Taking into account the stability interval, the interval of the imaginary axis contained in the stability region, and the radius of absolute monotonicity as functions of α (see Figure 13), and expressions (29) and (32), we can conclude that α should be close to $\frac{1}{2}(2 - \sqrt{3}) \approx 0.133975$. A choice that is compatible with this requirement is $\alpha = 5/36 \approx 0.138889$. For this value, the coefficients for the explicit scheme obtained so far are

$$\begin{array}{c|ccc} 0 & 0 & 0 & 0 \\ \frac{5}{6} & \frac{5}{6} & 0 & 0 \\ \frac{1}{3b_3} & \frac{1}{6b_3} & \frac{1}{6b_3} & 0 \\ \hline \mathcal{A} & \frac{4}{5} - b_3 & \frac{1}{5} & b_3 \end{array} \quad (33)$$

where b_3 is such that

$$\frac{1}{5} \leq b_3 \leq \frac{3}{5}. \quad (34)$$

For scheme (33), expression (32) is

$$\mathcal{R}_{Lin}(\mathbb{A}) = \mathcal{R}(\mathbb{A}) = \frac{6}{5}.$$

Furthermore, the interval $[-iw, iw] \subseteq \mathcal{S}$ for $w = 1.2$; the interval $[-z, 0] \subseteq \mathcal{S}$ for $z = 2.84745$, and $R(-z) \geq 0$ for $z \in [0, 1.81803]$. The stability region, and a zoom of the region close to the imaginary axis are given in Figure 1 (dotted line).

6.1.2. Implicit scheme

For the implicit scheme, the weight vector b is the same as the one for the explicit scheme. Thus, from the previous section, see (33) and (34), we have that

$$b_1 = \frac{4}{5} - b_3, \quad b_2 = \frac{1}{5}, \quad \frac{1}{5} \leq b_3 \leq \frac{3}{5}. \quad (35)$$

Condition (4) and second order conditions (3) for the implicit scheme lead to

$$\tilde{c}_3 = \frac{-2b_2\tilde{c}_2 + 2b_2\gamma + 2b_3\gamma - 2\gamma + 1}{2b_3}, \quad \tilde{c}_1 = \gamma, \quad (36)$$

$$\tilde{a}_{21} = \tilde{c}_2 - \gamma, \quad \tilde{a}_{31} = \tilde{c}_3 - \tilde{a}_{32} - \gamma. \quad (37)$$

Thus, the implicit scheme introduces three additional degrees of freedom to the combined scheme (2). We choose these as \tilde{c}_2 , \tilde{a}_{32} , and γ in the following. Since b_1 and b_2 are constrained by (35), it remains to constrain b_3 and thus a total of four degrees of freedom is left to be optimized for the implicit scheme.

Next, we study the stability function of the implicit scheme and impose conditions to obtain L -stability.

Stability function for the implicit scheme. As it has been pointed out in Section 1, we aim at constructing an L -stable method, that is, an A -stable method such that $\lim_{z \rightarrow \infty} R(z) = 0$. A detailed study of stability issues for SDIRK methods is given in [8, Chapter IV.6]. For SDIRK methods with $a_{11} = \dots = a_{ss} = \gamma$, the stability function is of the form

$$R(z) = \frac{P(z)}{Q(z)},$$

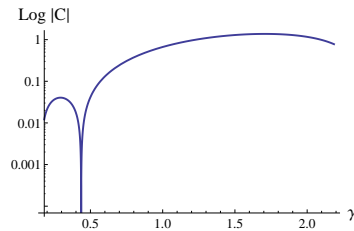


Figure 14: Error constant for second order 3-stage SDIRK methods.

where $P(z)$ is a polynomial of degree at most s , and $Q(z) = (1 - \gamma z)^s$. For these schemes, in the case $\gamma > 0$, A -stability is equivalent to

$$E(y) = |Q(iy)|^2 - |P(iy)|^2 \geq 0 \quad \text{for all } y \in \mathbb{R}. \quad (38)$$

For L -stable methods, $R(\infty) = 0$ and thus the highest coefficient of P is zero. Furthermore, if the method is known to be of order p , with $p \geq s - 1$, then the rest of the coefficients are uniquely determined in terms of s -degree Laguerre polynomials (see [8, Chapter IV.6, p. 105]).

These results can be applied to our method ($p = 2$ and $s = 3$). In this case, according to [8, Chapter IV.6], expression (38) is given by

$$E(y) = y^4 \left(-6\gamma^4 + 18\gamma^3 - 12\gamma^2 + 3\gamma - \frac{1}{4} \right) + y^6 \gamma^6, \quad (39)$$

and the stability function can be computed as

$$R(z) = \frac{z^2 (6\gamma^2 - 6\gamma + 1) + z(2 - 6\gamma) + 2}{2(1 - \gamma z)^3}. \quad (40)$$

The regions of γ for L -stability can be obtained imposing non negativity to the coefficients of $E(y)$ in (39); in this way we obtain that the parameter γ should satisfy

$$\frac{1}{12} \left(9 + 3\sqrt{3} - \sqrt{6(12 + 7\sqrt{3})} \right) \leq \gamma \leq \frac{1}{4} \left(3 + \sqrt{3} + \sqrt{8 + \frac{14}{\sqrt{3}}} \right),$$

whose numerical approximations (see [8, Chapter IV.6, Table 6.4]) are given by

$$0.18042531 \leq \gamma \leq 2.18560010. \quad (41)$$

For second order 3-stage L -stable SDIRK schemes, the error constant is also known in terms of the 3-degree Laguerre polynomial $L_3(x)$ (see [8, Chapter IV.6, p. 105]),

$$C = -L_3 \left(\frac{1}{\gamma} \right) \gamma^3 = -\gamma^3 + 3\gamma^2 - \frac{3\gamma}{2} + \frac{1}{6},$$

and third order is obtained for $\gamma = 0.43586652$. In Figure 14 we show the values of $\log |C|$.

If we compute the function $E(y)$ from the Butcher tableau of the SDIRK method, and we use the values of $b_1, b_2, \tilde{c}_3, \tilde{c}_1, \tilde{a}_{21}$, and \tilde{a}_{31} given by (35)–(37), we obtain that the function $E(y)$ is of the form (39) if

$$\tilde{c}_2 = \frac{2\tilde{a}_{32}b_3\gamma + 2\gamma^3 - 4\gamma^2 + \gamma}{2\tilde{a}_{32}b_3}. \quad (42)$$

For this value, the stability function computed from the Butcher tableau is (40).

At this point, we recall that the coefficients of the SDIRK method should be positive. With the value of \tilde{c}_2 given by (42), the coefficient \tilde{a}_{21} in (37) is

$$\tilde{a}_{21} = \frac{\gamma(2\gamma^2 - 4\gamma + 1)}{2\tilde{a}_{32}b_3}.$$

If we impose that $\tilde{a}_{21} > 0$ and take into account (41), we obtain that γ must satisfy

$$0.180425 \leq \gamma \leq \frac{1}{2}(2 - \sqrt{2}) \quad \text{or} \quad \frac{1}{2}(2 + \sqrt{2}) \leq \gamma \leq 2.1856.$$

As $\frac{1}{2}(2 - \sqrt{2}) \approx 0.29289322$ and $\frac{1}{2}(2 + \sqrt{2}) \approx 1.70710678$, taking into account the size of the error constant (see Figure 14), we restrict the values of γ for L -stability in (41) to

$$0.18042531 \leq \gamma \leq 0.29289322. \quad (43)$$

Note that this interval does not contain the value of γ for which the scheme would be of third order.

With regard to the intersection of the real and imaginary axis with the stability region, observe that, as the method is L -stable, the imaginary axis as well as the real axis are contained in the stability region \mathcal{S} . It remains to study the non negativity of the stability function.

We analyze now if there is any value of γ such that $R(z) \geq 0$ for all $z < 0$. We obtain a positive answer for

$$\gamma \in \left(0, \frac{1}{3}(3 - \sqrt{6})\right] \approx (0, 0.18350342]. \quad (44)$$

Combining this result with (43), we get that adequate values for γ are

$$0.18042531 \leq \gamma \leq 0.18350342. \quad (45)$$

Radius of absolute monotonicity for linear problems. For linear problems, the computation of the radius of absolute monotonicity for implicit schemes is not an easy task. To obtain it, we have to find the points z such that the stability function R is absolutely monotonic at z . Recall that a function f is said to be absolutely monotonic at a given point $x \in \mathbb{R}$ if $f^{(k)}(x)$ exists and $f^{(k)}(x) \geq 0$ for $k \geq 0$. For explicit methods, the stability function R is a polynomial, and thus, we can analyze a finite number of derivatives to check if the function is absolutely monotonic at a given point x . However, for implicit schemes, R is a rational function, and we cannot use directly the definition of absolute monotonicity.

To obtain the radius of absolute monotonicity for linear problems for our SDIRK method, we apply Theorem 4.4 in [7]. Roughly speaking, this result allows us to restrict the analysis to a finite number of derivatives, that is, $R^{(k)}(x) \geq 0$ for $0 \leq k < K(x)$, and the key point is to obtain the integer $K(x)$. In the following proposition we compute it for the stability function (40).

Proposition 6.1. *Assume that γ satisfies (45). If $R^{(k)}(x) \geq 0$ for $k = 0, 1, 2, 3$, then the stability function (40) is absolutely monotonic at x .*

Proof. In order to apply [7, Theorem 4.4], we construct all the elements (sets, intervals, functions, etc.) involved in this result. Following the notation in [7], the stability function (40) is of the form $R(z) = P(z)/Q(z)$ with

$$P(z) = \left(3\gamma^2 - 3\gamma + \frac{1}{2}\right)z^2 + (1 - 3\gamma)z + 1, \quad Q(z) = \gamma^3 \left(\frac{1}{\gamma} - z\right)^3.$$

The polynomials P and Q have degrees $m = 2$ and $n = 3$, respectively, and there is a unique pole $\alpha_0 = 1/\gamma > 0$ with multiplicity $\mu(\alpha_0) = 3$. Thus the set $A = A^+ = \{\alpha_0\}$, $I(\alpha_0) = \mathbb{R}$, and $B(R(z)) = \infty$. Next, the stability function should be decomposed into partial fractions of the form

$$R(z) = c(\alpha_0, 1) \frac{1}{\alpha_0 - z} + c(\alpha_0, 2) \frac{1}{(\alpha_0 - z)^2} + c(\alpha_0, 3) \frac{1}{(\alpha_0 - z)^3}.$$

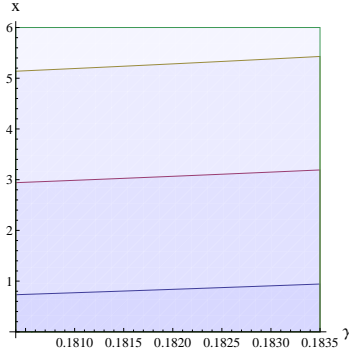


Figure 15: From bottom to top, values of $-x$ such that condition (46) holds for $k = 1, 2, 3, 4$.

In our case,

$$c(\alpha_0, 1) = \frac{6\gamma^2 - 6\gamma + 1}{2\gamma^3}, \quad c(\alpha_0, 2) = \frac{-3\gamma^2 + 5\gamma - 1}{\gamma^4}, \quad c(\alpha_0, 3) = \frac{2\gamma^2 - 4\gamma + 1}{2\gamma^5}.$$

For γ satisfying (45), these functions have constant sign. More precisely, $c(\alpha_0, 1) > 0$, $c(\alpha_0, 2) < 0$, and $c(\alpha_0, 3) > 0$. Now, we construct the function (see [7, Formula (4.2)])

$$F(k, x) = \frac{2c(\alpha_0, 1)k!}{(k+2)!} \left(\frac{1}{\gamma} - x\right)^2 - \frac{2c(\alpha_0, 2)(k+1)!}{(k+2)!} \left|\frac{1}{\gamma} - x\right|,$$

where we have used the sign conditions of $c(\alpha_0, 1)$ and $c(\alpha_0, 2)$. Another function needed to construct $K(x)$ in [7] is $L(x)$; in our case, $L(x) = 0$, see [7, Formula (4.3)]. We can now construct the integer $K(x)$ in [7, Definition 4.1]), defined as the smallest integer k such that $k \geq L(x)$ and

$$F(k, x) < |c(\alpha_0, 3)|. \quad (46)$$

For γ satisfying (45), in Figure 15 we show, from bottom to top, the values of $-x$ such that condition (46) holds for $k = 1, 2, 3, 4$. We do not consider $k = 0$ because, as we have seen above (see (44)), for the values of γ satisfying (45), it holds that $R(z) \geq 0$ for $z \leq 0$. Furthermore, we restrict the values to $-x \in [0, 6]$ because, by numerical search, it has been found that the optimum radius of absolute monotonicity for second order 3-stage SDIRK schemes is equal to 6 [3, 18]. Consequently, for $-x \in [0, 6]$, $K(x) \leq 4$. We can now apply Theorem 4.4 in [7] to ensure that $R(z)$ is absolutely monotonic in $[x, 0]$ if and only if $c(\alpha_0, 3) > 0$ and $R^{(k)}(x) \geq 0$ for $0 \leq k < K(x)$. As $K(x) \leq 4$, we obtain the desired result. \square

The next step is to analyze the values of x such that $R^{(k)}(x) \geq 0$ for $k = 0, 1, 2, 3$. For each γ satisfying (45), the radius of absolute monotonicity is given by

$$\mathcal{R}(\gamma) = \frac{1 - 4\gamma}{\gamma(6\gamma^2 - 6\gamma + 1)} - \sqrt{\frac{-12\gamma^3 + 28\gamma^2 - 10\gamma + 1}{\gamma^2(6\gamma^2 - 6\gamma + 1)^2}}, \quad (47)$$

and varies in the interval $[4.25512, 4.44949]$. In Figure 16 we show, for each γ , the interval of absolute monotonicity, and a zoom of the value range of the radius of absolute monotonicity. We observe that, for the different values of γ , the radius of absolute monotonicity does not change significantly.

Uniform convergence for IMEX RK methods. Condition (6) seems to be of interest when stiff systems of the form (5) are solved. For this reason, we impose the implied relationship

$$\tilde{a}_{32} = \frac{3\gamma - 6\gamma^2}{5b_3}. \quad (48)$$

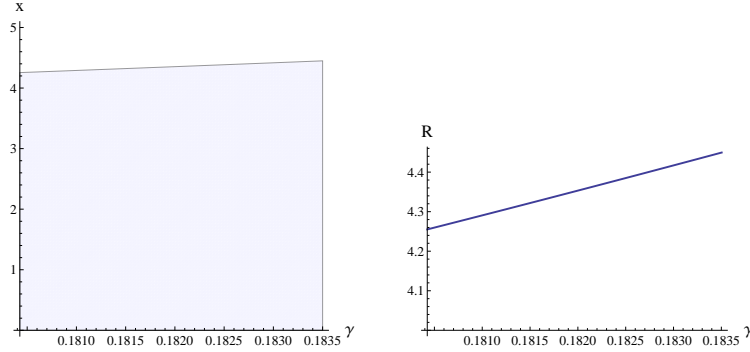


Figure 16: Left: Interval of absolute monotonicity. Right: zoom of the range values of the radius of absolute monotonicity.

Choice of γ . Based on the analysis done so far, now we choose the value of γ satisfying (45). If we rationalize the mid point, 0.1819643628, we obtain

$$\gamma = \frac{2}{11} \approx 0.181818. \quad (49)$$

At this point, it remains to obtain the parameter b_3 ; recall from (35) that this value should satisfy

$$\frac{1}{5} \leq b_3 \leq \frac{3}{5}. \quad (50)$$

We still have to deal with the Kraaijevanger's coefficient for nonlinear problems for the SDIRK method, and with the region of absolute monotonicity for the IMEX RK method.

Absolute monotonicity for the SDIRK and IMEX RK schemes. We determine b_3 satisfying (50) to obtain a large Kraaijevanger's coefficient for the SDIRK method, and a large region of absolute monotonicity for the IMEX RK scheme.

From (9), a study of the Kraaijevanger's coefficient $\mathcal{R}(\tilde{\mathbb{A}})$ for the SDIRK method yields that the largest value possible is $\mathcal{R}(\tilde{\mathbb{A}}) = 42/11 \approx 3.8181$, and this value is attained for any b_3 such that

$$\frac{4066}{11275} \leq b_3 \leq \frac{4463}{11275} \quad (0.360621 \leq b_3 \leq 0.395831). \quad (51)$$

Considering the points (r_1, r_2) in the region of absolute monotonicity $\mathcal{R}(\mathbb{A}, \tilde{\mathbb{A}})$, when $r_1 = 0$ (or $r_2 = 0$), we obtain the point $(0, r_2)$ (or $(r_1, 0)$), that is, the intersection of the region of absolute monotonicity with the axis $r_1 = 0$ (axis $r_2 = 0$). These values satisfy $r_2 \leq \mathcal{R}(\tilde{\mathbb{A}})$, $r_1 \leq \mathcal{R}(\mathbb{A})$. Quite often, due to the mixed conditions (10) for $r_1 = 0$, and (11) for $r_2 = 0$, that is,

$$(I + r_2 \tilde{\mathbb{A}})^{-1} \mathbb{A} \geq 0, \quad (I + r_1 \mathbb{A})^{-1} \tilde{\mathbb{A}} \geq 0,$$

we obtain $r_2 < \mathcal{R}(\tilde{\mathbb{A}})$ and $r_1 < \mathcal{R}(\mathbb{A})$. We aim at determining the largest values of r_2 and r_1 such that the points $(r_1, 0)$ and $(0, r_2)$ belong to the region of absolute monotonicity. A detailed study yields the result that the largest value of r_2 such that $(0, r_2) \in \mathcal{R}(\mathbb{A}, \tilde{\mathbb{A}})$ is $r_2 = 66/43 \approx 1.53488$, provided that

$$\frac{1}{5} \leq b_3 \leq \frac{1462}{3025} \quad (0.2 \leq b_3 \leq 0.483306). \quad (52)$$

In a similar way, the largest value of r_1 such that $(r_1, 0) \in \mathcal{R}(\mathbb{A}, \tilde{\mathbb{A}})$ is $r_1 = 126/55 \approx 2.29091$, provided that

$$\frac{1}{5} \leq b_3 \leq \frac{109616}{213565} \quad (0.2 \leq b_3 \leq 0.513268). \quad (53)$$

Taking into account (51), (52), and (53), we consider

$$b_3 = \frac{4}{11} \approx 0.363636. \quad (54)$$

By fixing this value, we have finished the construction of the IMEX RK scheme (17).

6.2. IMEX methods with second order 3-stage optimum SSP explicit RK scheme as explicit method

In the previous section we have constructed a second order 3-stage IMEX RK method with all the properties pointed out in the introduction, amongst them, a nontrivial intersection of the stability region of the explicit RK method and the imaginary axis. It turns out that this property of the explicit scheme leads to an important decrease of the stability interval, the interval of non negativity of the stability function, and the Kraaijevanger's coefficient. For this reason, in this section, we construct SSP IMEX RK methods, based on the optimal explicit 3-stage second-order method in conjunction with a compatible implicit scheme.

Thus, we consider IMEX RK schemes of the form

$$\begin{array}{c|ccc} 0 & 0 & 0 & 0 & \tilde{c}_1 & \gamma & 0 & 0 \\ \frac{1}{2} & \frac{1}{2} & 0 & 0 & \tilde{c}_2 & \tilde{a}_{21} & \gamma & 0 \\ 1 & \frac{1}{2} & \frac{1}{2} & 0 & \tilde{c}_3 & \tilde{a}_{31} & \tilde{a}_{32} & \gamma \\ \hline \mathcal{A} & \frac{1}{3} & \frac{1}{3} & \frac{1}{3} & \tilde{\mathcal{A}} & \frac{1}{3} & \frac{1}{3} & \frac{1}{3} \end{array} \quad (55)$$

The explicit method coincides with the explicit scheme for the SSP2(3,3,2) schemes in [11, 25] (see too (60)). Observe that now, the weight vector b for the implicit scheme is already fixed. Recalling the discussion from Section 6.1.2, see (36)-(37), we note that this leaves only three degrees of freedom for the scheme (55), namely, \tilde{c}_2 , \tilde{a}_{32} , and γ .

For the implicit schemes considered in this section, we will impose L -stability and the non negativity of the stability function $R(z)$ for all $z \leq 0$. As the stability function for an L -stable second order 3-stage SDIRK method only depends on the diagonal elements γ , the study conducted in Section 6.1.2 is valid and, therefore, we choose again $\gamma = 2/11$.

Furthermore, after imposing second order conditions for the implicit scheme, and a stability function of the form (40) with $\gamma = 2/11$, the value of \tilde{c}_2 is also determined, and we obtain that there is one free parameter left: \tilde{a}_{32} . In this section, we construct three schemes by choosing this value as follows: in Section 6.2.1 we impose condition (6) for uniform convergence, in Section 6.2.2 we optimize the Kraaijevanger's coefficient of the SDIRK scheme, and in Section 6.2.3 we optimize the region of absolute monotonicity of the IMEX RK scheme.

Recall that for all the schemes constructed in this section, the stability function for the explicit scheme is (21) whereas for the implicit scheme it is given by $R_{\tilde{\mathcal{A}}}(z)$ in (18), since it depends only on γ (see (40)).

6.2.1. IMEX RK method with uniform convergence (6)

In this case, by imposing (6) we get $\tilde{a}_{32} = 42/121$, and the IMEX RK scheme obtained is given by the coefficient tableaux (20). Note that (48) must not be reused to obtain \tilde{a}_{32} because (48) has been derived assuming (35) where $b_2 = 1/5$ instead of $b_2 = 1/3$.

6.2.2. IMEX RK scheme with large radius of absolute monotonicity $\mathcal{R}(\tilde{\mathcal{A}})$

A detailed study shows that the largest value for $\mathcal{R}(\tilde{\mathcal{A}})$ is 3.85824, and that this value is attained for $\tilde{a}_{32} = 0.3039$. We rationalize this number to obtain

$$\tilde{a}_{32} = \frac{7}{23} \approx 0.304348.$$

We thus obtain the IMEX RK scheme (22). We remark that this method does not satisfy condition (6) for uniform convergence.

6.2.3. IMEX RK scheme with large region of absolute monotonicity

A detailed study shows that the largest value of r_2 such that $(0, r_2) \in \mathcal{R}(\mathbb{A}, \tilde{\mathbb{A}})$ is $r_2 = 2.34236$; this value is attained for $\tilde{a}_{32} = 0.47635$. We rationalize this number to obtain that for

$$\tilde{a}_{32} = \frac{10}{21} \approx 0.47619,$$

we have that the point $(0, r_2)$ is in the region of absolute monotonicity for

$$r_2 = \frac{11(\sqrt{9242421} - 2641)}{1874} \approx 2.34284.$$

We thus obtain the IMEX RK scheme (23). We remark that this method does not satisfy condition (6) for uniform convergence.

7. Appendix B: IMEX schemes from the literature

In this section we give the coefficients of different methods from the literature used in the paper, whose properties are given in Table 6.

- IMEX SSP1(1,1,1)–LPM method:

$$\begin{array}{c|c} 0 & 0 \\ \hline \mathcal{A} & 1 \end{array} \quad \begin{array}{c|c} 1 & 1 \\ \hline \tilde{\mathcal{A}} & 1 \end{array} \quad (56)$$

- IMEX ARS(1,1,1)–LPUM method:

$$\begin{array}{c|cc} 0 & 0 & 0 \\ 1 & 1 & 0 \\ \hline \mathcal{A} & 1 & 0 \end{array} \quad \begin{array}{c|cc} 0 & 0 & 0 \\ 1 & 0 & 1 \\ \hline \tilde{\mathcal{A}} & 0 & 1 \end{array} \quad (57)$$

- IMEX SSP2(2,2,2)

$$\begin{array}{c|cc} 0 & 0 & 0 \\ 1 & 1 & 0 \\ \hline \mathcal{A} & \frac{1}{2} & \frac{1}{2} \end{array} \quad \begin{array}{c|cc} \gamma & \gamma & 0 \\ 1-\gamma & 1-2\gamma & \gamma \\ \hline \tilde{\mathcal{A}} & \frac{1}{2} & \frac{1}{2} \end{array} \quad (58)$$

that will be named SSP2(2,2,2)–PM for $\gamma = 0.24$ [21], and SSP2(2,2,2)–LM for $\gamma = 1 - 1/\sqrt{2}$ [25].

- SSP2(2,2,2)–UM (see, e.g., [16, Example 4.8]):

$$\begin{array}{c|cc} 0 & 0 & 0 \\ 1 & 1 & 0 \\ \hline \mathcal{A} & 1/2 & 1/2 \end{array} \quad \begin{array}{c|cc} 0 & 0 & 0 \\ 1 & 1/2 & 1/2 \\ \hline \tilde{\mathcal{A}} & 1/2 & 1/2 \end{array} \quad (59)$$

- IMEX SSP2(3,3,2)–LUM method ([11]; see also[21]):

$$\begin{array}{c|ccc} 0 & 0 & 0 & 0 \\ \frac{1}{2} & \frac{1}{2} & 0 & 0 \\ 1 & \frac{1}{2} & \frac{1}{2} & 0 \\ \hline \mathcal{A} & \frac{1}{3} & \frac{1}{3} & \frac{1}{3} \end{array} \quad \begin{array}{c|ccc} \frac{1}{5} & \frac{1}{5} & 0 & 0 \\ \frac{3}{10} & \frac{1}{10} & \frac{1}{5} & 0 \\ 1 & \frac{1}{3} & \frac{1}{3} & \frac{1}{3} \\ \hline \tilde{\mathcal{A}} & \frac{1}{3} & \frac{1}{3} & \frac{1}{3} \end{array} \quad (60)$$

Method		$[-iw, iw]$	$[-w, 0]$	$R(-z) \geq 0$	\mathcal{R}_{Lin}	\mathcal{R}	A/L-stable	(6)
(56) SSP1(1,1,1)–LPM	Exp.	$w = 0$	$w = 2$	$z = 1$	1	1		No
	Imp.	$w = \infty$	$w = \infty$	$z = \infty$	∞	∞	L -stable	
(57) ARS(1,1,1)–LPUM	Exp.	$w = 0$	$w = 2$	$z = 1$	1	1		Yes*
	Imp.	$w = \infty$	$w = \infty$	$z = \infty$	∞	∞	L -stable	
(58) $\gamma = 1 - 1/\sqrt{2}$ SSP2(2,2,2)–LM	Exp.	$w = 0$	$w = 2$	$z = \infty$	1	1		No
	Imp.	$w = \infty$	$w = \infty$	$z = 2.41$	2.41	2.41	L -stable	
(58) $\gamma = 0.24$ SSP2(2,2,2)–PM	Exp.	$w = 0$	$w = 2$	$z = \infty$	1	1		No
	Imp.	$w = \infty$	$w = 50$	$z = \infty$	3.57	3.57		
(59) SSP2(2,2,2)–UM	Exp.	$w = 0$	$w = 2$	$z = \infty$	1	1		Yes*
	Imp.	$w = \infty$	$w = \infty$	$z = 2$	2	2	A -stable	
(60) SSP2(3,3,2)–LUM	Exp.	$w = 0$	$w = 4.52$	$z = 3.59$	2	2		Yes
	Imp.	$w = \infty$	$w = \infty$	$z = 2.43$	2.43	2.43	L -stable	

Table 6: Properties of IMEX RK methods (56)–(60). The last column denotes whether the uniform convergence condition (6) is fulfilled. For the meaning of ‘Yes*’ see Note 7.1

Note 7.1. For schemes (57) and (59) the coefficient matrix for the implicit method is singular and thus condition (6) cannot be applied. For these schemes we have considered condition (6) for the method

$$\begin{array}{c|cc} \varepsilon & \varepsilon & 0 \\ c & a & \hat{A} \\ \hline & b_1 & \hat{b} \end{array}$$

and we have taken $\varepsilon \rightarrow 0$.

- [1] S. Boscarino, Error analysis of IMEX Runge–Kutta methods derived from differential–algebraic systems, *SIAM J. Numer. Anal.* 45 (2008) 1600–1621.
- [2] L. Ferracina, M. Spijker, An extension and analysis of the Shu–Osher representation of Runge–Kutta methods, *Math. Comp.* 74 (2004) 201–219.
- [3] L. Ferracina, M. Spijker, Strong stability of singly-diagonally-implicit Runge–Kutta methods, *Appl. Numer. Math.* 58 (2008) 1675–1686.
- [4] S. Gottlieb, D. Ketcheson, C.W. Shu, High order strong stability preserving time discretizations, *J. Sci. Comput.* 38 (2009) 251–289.
- [5] S. Gottlieb, C.W. Shu, Total variation diminishing Runge–Kutta schemes, *Math. Comp.* 67 (1998) 73–85.
- [6] S. Gottlieb, C.W. Shu, E. Tadmor, Strong stability-preserving high-order time discretization methods, *SIAM Rev.* 43 (2001) 89–112.
- [7] J. Van de Griend, J. J. Kraaijevanger, Absolute monotonicity of rational functions occurring in the numerical solution of initial value problems, *Numer. Math.* 49 (1986) 413–424.
- [8] E. Hairer, G. Wanner, *Solving Ordinary Differential Equations II*, Springer-Verlag, Berlin–Heidelberg–New York, 1991.
- [9] I. Higuera, On strong stability preserving time discretization methods, *J. Sci. Comput.* 21 (2004) 193–223.
- [10] I. Higuera, Representations of Runge–Kutta methods and strong stability preserving methods, *SIAM J. Numer. Anal.* 43 (2005) 924–948.
- [11] I. Higuera, Strong stability for additive Runge–Kutta methods, *SIAM J. Numer. Anal.* 44 (2006) 1735–1758.
- [12] I. Higuera, Characterizing strong stability preserving additive Runge–Kutta methods, *J. Sci. Comput.* 39 (2009) 115–128.
- [13] I. Higuera, O. Rey, Imex time-stepping methods for the black-scholes equation, in preparation (2013).
- [14] W. Hundsdorfer, S.J. Ruuth, Imex extensions of linear multistep methods with general monotonicity and boundedness properties, *J. Comput. Phys.* 225 (2007) 2016–2042.
- [15] W. Hundsdorfer, M. Spijker, Boundedness and strong stability of Runge–Kutta methods, *Math. Comp.* 80 (2011) 863–886.
- [16] W. Hundsdorfer, J.G. Verwer, *Numerical Solution of Time-Dependent Advection-Diffusion-Reaction Equations*, Springer, 2003.
- [17] A. Iserles, *A first course in the numerical analysis of differential equations*, Cambridge University Press, 1996.
- [18] D. Ketcheson, C. MacDonald, S. Gottlieb, Optimal implicit strong stability preserving Runge–Kutta methods, *Appl. Numer. Math.* 59 (2009) 373–392.
- [19] J. Kraaijevanger, Contractivity of Runge–Kutta methods, *BIT* 31 (1991) 482–528.

- [20] J.F.B.M. Kraaijevanger, Absolute monotonicity of polynomials occurring in the numerical solution of initial value problems, *Numer. Math.* 48 (1986) 303–322.
- [21] F. Kupka, N. Happenhofer, I. Higuera, O. Koch, Total-variation-diminishing implicit-explicit Runge-Kutta methods for the simulation of double-diffusive convection in astrophysics, *J. Comput. Phys.* 231 (2012) 3561–3586.
- [22] J. Leconte, G. Chabrier, A new vision of giant planet interiors: impact of double diffusive convection, *Astronomy and Astrophysics* 540 (2012) A20.
- [23] M. Motamed, C. Macdonald, S. Ruuth, On the linear stability of the fifth-order WENO discretization, *J. Sci. Comput.* 47 (2011) 127–149.
- [24] H. Muthsam, F. Kupka, B. Löw-Baselli, C. Obertscheider, M. Langer, P. Lenz, ANTARES — A Numerical Tool for Astrophysical REsearch with applications to solar granulation, *New Astronomy* 15 (2010) 460–475.
- [25] L. Pareschi, G. Russo, Implicit-explicit Runge-Kutta schemes and application to hyperbolic systems with relaxation, *J. Sci. Comput.* 25 (2005) 129–155.
- [26] C.W. Shu, Total-variation-diminishing time discretizations, *SIAM J. Sci. Statist. Comput.* 9 (1988) 1073–1084.
- [27] C.W. Shu, A survey of strong stability-preserving high-order time discretization methods, in: *Collected Lectures on the Preservation of Stability under Discretization*, SIAM, Philadelphia, PA, 2002, pp. 51–65.
- [28] M. Spijker, Contractivity in the numerical solution of initial value problems, *Numer. Math.* 42 (1983) 271–290.
- [29] M. Spijker, Step size restrictions for stability of one-step methods in the numerical solution of initial value problems, *Math. Comp.* 45 (1985) 377–392.
- [30] M. Spijker, Step size conditions for general monotonicity in numerical initial value problems, *SIAM J. Numer. Anal.* 45 (2007) 1226–1245.
- [31] J. Strikwerda, *Finite Difference Schemes and Partial Differential Equations*, 2nd ed., SIAM, Philadelphia, PA, 2004.
- [32] R. Wang, R. Spiteri, Linear instability of the fifth-order WENO method, *SIAM J. Numer. Anal.* 45 (2007) 1871–1901.
- [33] F. Zaussinger, Numerical simulation of double-diffusive convection, Ph.D. thesis, University of Vienna, 2010. Available at <http://othes.univie.ac.at/13172/>.
- [34] F. Zaussinger, H. Spruit, Semiconvection: numerical simulations, *Astronomy and Astrophysics* 554 (2013) A119.